AD-A173 306 BLUE-GREEN LASER DIODE RESEARCH PROGRAM(U) MINNESOTA MINING AND MFG CO ST PAUL ELECTRONIC AND INFORMATION SECTOR LAB JUL 86 N00014-85-C-0552 1/1

UNCLASSIFIED F/G 20/12 NL

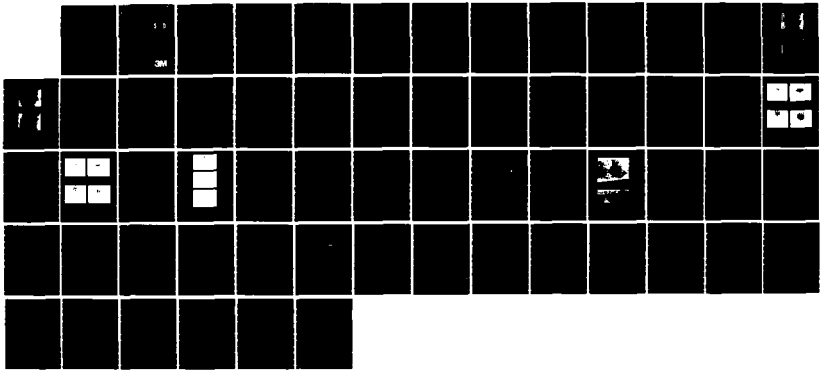

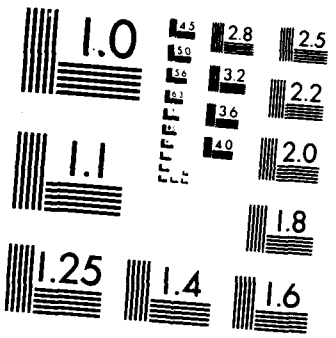

BLUE-GREEN LASER DIODE RESEARCH PROGRAM

Quarterly Technical Progress Report No. 1
For The Period April 1, 1986 To June 30, 1986

Prepared Under
Contract Number N00014-85-C-0552

JULY, 1986

The views and conclusions contained in this document are those of the authors and should not be interpreted as necessarily representing the official policies, either expressed or implied, of the Defense Advanced Research Projects Agency or the U.S. Government.

Work supported in part by the:

DEFENSE ADVANCED RESEARCH PROJECTS AGENCY
1400 Wilson Boulevard
Arlington, VA 22209

Under the:

OFFICE OF NAVAL RESEARCH
Department Of The Navy
800 N. Quincy Street
Arlington, VA 22217-5000

Electronic and Information
Sector Laboratories/3M
St. Paul, MN 55144

3M

EXECUTIVE SUMMARY

A total of 24 heteroepitaxial films of ZnSe on GaAs were grown in the St. Paul laboratory during the reporting period. A range of ratios of the Zn beam pressure to the Se beam pressure during growth (the BPR), and a range of substrate temperatures during growth, were investigated in order to determine the set of growth conditions giving the best intrinsic films. The term "best" is defined as the largest near-band-edge emission observed in photoluminescence, combined with the highest peak mobility, lowest room temperature carrier density, and lowest total concentration of ionized impurities. While the series of films has not yet been completed, it appears that a BPR of 1:1 and a substrate temperature of 350°C give the best intrinsic films. Preliminary evidence suggests that the surface quality of the films begins to degrade after exposure to room ambient for about two weeks.

The six-month report for this project described the first attempts to grow ZnSe epitaxially on Ge substrates. This work has been expanded to include an epitaxial buffer layer of Ge between the ZnSe layer and the Ge substrate. This was done to provide a smoother substrate for the ZnSe growth. RHEED patterns indicate that ZnSe films grown on the Ge buffer layer are indeed smoother on the atomic scale. Photoluminescence results show that the near-band-edge emission is much stronger than for films without a buffer layer. The PL peak known as $I_1^{d \bullet \bullet p}$ grows in intensity as the buffer layer thickness is increased. This peak is also very narrow.

TEM studies of a number of ZnSe on GaAs films grown at different BPR have shown that the BPR seems uncorrelated with defect formation in the films. For very thin films (less than 0.2 micron) TEM shows that the substrate-film interface is smooth. However for thicker films, a periodic strain field was found along the interface, presumably due to misfit dislocations. This result is confirmed by double crystal X-ray results. In these experiments very thin films were seen to be tetragonally distorted, while films thicker than about 0.4-0.5 micron were cubic. It thus appears that a "critical" thickness of about 0.4 micron exists, below which the films are coherent with the substrate and relatively defect-free, and above which they have bulk lattice parameters and physical defects.

Work has continued on using SIMS analyses to investigate the chemical quality of the ZnSe films. Primary emphasis has been on detection of Ga and In impurities because both elements are present in the growth process. While SIMS results are always somewhat uncertain, numerically it does appear that the maximum Ga concentration is between 20 and 200 times less than the donor concentration at room temperature, depending on the sample. The maximum In concentration is between 200 and 3000 times lower than the donor concentration. Preliminary attempts have been made to detect Al, with results showing in all cases that the Al concentration is between 2 and 200 times less than the donor concentration.

Electron beam pumped lasing action in epitaxial ZnSe has continued to be studied. Threshold current density and lasing wavelength have been studied as functions of sample temperature. The lasing wavelength was found to vary more rapidly with T than expected from the temperature dependence of the band-gap. The overall efficiency of the lasing process (as estimated from light power out/electron beam power in) was about 1.5%.

TABLE OF CONTENTS

LIST OF FIGURES

LIST OF FIGURES (Cont.)

LIST OF TABLES

1.0 INTRODUCTION

This report covers progress during the seventh through ninth months of ONR Contract N00014-85-C-0552. The various sections of the report are numbered and titled using the format of the original proposal. As before, results from parallel programs at 3M-St. Paul (ZnSe on GaAs substrates) and 3M-Canada (ZnSe on Ge substrates) are discussed.

2.0 PROGRESS REPORT

2.1 Project I, Task 1: Materials Research - Undoped ZnSe Research

Unintentionally doped ZnSe layers are being grown by molecular beam epitaxy in order to understand the nature of native defects in the layers and at the heterointerface, as well as to understand and quantify the contributions of these native defects and source material impurities to the carrier concentration.

During the past three months of the contract period, the effort in St. Paul has continued to be in the epitaxial growth of ZnSe on (100)GaAs, and the Toronto effort has concentrated on ZnSe grown on (100)Ge substrates with Ge buffer layers of various thicknesses. Some preliminary work has also been done in Toronto on the growth of ZnSe on (211)Ge substrates.

2.1.1. ZnSe Heteroepitaxy on (100)GaAs

During the past three months, 24 unintentionally doped ZnSe layers (ZSE23 to ZSE46) were grown on GaAs substrates (N^+ and semi-insulating). This is part of the on-going study to determine the proper substrate preparation and growth procedures to obtain high-quality undoped ZnSe layers. The important variables involved in these procedures include the desorption temperature of the GaAs substrate, the As overpressure during the substrate desorption, and the Zn-to-Se beam pressure ratio (BPR) and substrate temperature (T_s) during the growth run. So far, the study has focused on the beam pressure ratio and the substrate temperature. The criteria used to judge the quality of the films are smooth surface morphology, good band edge emission in photoluminescence (PL), low carrier and ionized impurity concentrations, and high carrier mobility of the layers. For clarity, these 24 growth runs will be discussed in 3 groups: namely, ZSE23 to ZSE29, ZSE30 to ZSE36, and ZSE37 to ZSE46.

2.1.1.1. The Growth of ZnSe Epitaxial layers on (100)GaAs

A. **Group 1 (ZSE23 to ZSE29)** - GaAs substrates were desorbed with an As overpressure to determine whether or not As flooding reduces the possible Ga outdiffusion from the substrate with a consequent reduction in the net donor concentration. All the layers were grown at a substrate temperature of 350°C. The BPR (Beam Pressure Ratio) was varied from 4 for ZSE23 to about 0.3 for ZSE29. No systematic change in the PL spectra was found. Note, however, that during the growth of these samples, measurements of the beam equivalent pressure were not reliable because of a memory effect in the nude ion gauge. This memory effect is partly due to the system design in which the nude ion gauge used for flux measurements prior to growth is left exposed to the fluxes during growth. Nonetheless, by using a proper flux measurement procedure, satisfactory results can be obtained. The ultimate solution would evidently be to protect the gauge with a shutter when it is not in use. Although a systematic trend was not seen in the results of PL and electrical measurements, such a trend was observed in the surface morphology of the layers. In general, the surface became rougher and the ZnSe overgrowth increased as the BPR was increased. The reason for increasing overgrowth at higher BPR is not yet clear.

B. **Group 2 (ZSE30 to ZSE36)** - The series of layers grown after reloading the sources and baking the system were for the purpose of investigating the effect on layer quality of new source material, as well as to check reproducibility from run-to-run and from day-to-day. Of the seven layers examined, the first four were grown in two days (two each day) using the same source ovens and substrate temperature settings. There was an apparent large increase in the Se flux and a slight change in the Zn flux. The reason for the dramatic increase in the Se flux is due to the change of the Se source from a full-load of small pellets into a half-full solid chunk, and a possible temperature gradient along the pyrolitic boron nitride (PBN) crucible. In addition, the PL peak in the excitonic region is observed to shift from lower energies to the normal position with a concomitant narrowing of the peak from about 11meV to 2meV as more material is consumed (refer to the PL results). The low intensity, broad emission peak is possibly due to the contamination on the surface of the source materials. The above observations suggest that thorough outgassing of source materials is very critical to obtaining high-quality layers. In addition, the reshaping of the Se source into a solid piece is necessary to

obtain a stable Se flux if the operating temperature of the Se oven is close to the melting temperature. Specimens ZSE34 and ZSE35 were grown under the same conditions as ZSE33 on two different days. The results of optical and electrical measurements are discussed elsewhere in this report.

C. **Group 3 (ZSE37 to ZSE46)** - These samples were grown to investigate the influence of BPR and T_s on surface morphology, and on the optical and electrical characteristics of the ZnSe layers. The BPR and T_s selected were 0.25, 0.5, 1, 2 and 250, 300, 350, 400°C, respectively, for a total of 16 combinations of growth conditions. Preliminary optical and electrical results are presented and discussed elsewhere in this report. Table 2-1 summarizes the present status of this group.

D. **Surface aging of MBE-grown ZnSe films** - Figure 2-1 shows two micrographs of the ZnSe surface at the same defect area under dark-field illumination, one taken immediately after removal of the sample from the MBE system (a), and one taken after three months storage in the room ambient (b). The density of small bright spots has increased during this period. The interference contrast micrographs remain essentially the same as shown in Figure 2-2. The bright straight lines are possibly due to surface damage incurred during stylus surface profiling. Three pieces of specimen from the same growth run were stored in different ambients (room ambient, moisture-free, and high vacuum) to investigate the possible cause of surface degradation. Preliminary results indicate that surface degradation of the specimen stored in the room ambient starts about two weeks after removal from the system. The influence of such degradation on optical and electrical properties will be investigated.

2.1.1.2 Photoluminescence Measurements On ZnSe/(100)GaAs

Photoluminescence measurements have been made at 9K and 300K on samples ZSE23-ZSE46. Samples in the series ZSE22-ZSE29 were plagued by reproducibility problems arising from problems with measuring and/or controlling the Se flux during growth. PL measurements on these samples did not show the trends we had come to expect based on earlier samples. After ZSE29, the MBE chamber was opened for reloading of source materials. On closing the system, we undertook a growth series to test for recovery of the

TABLE 2-1. Results Of Electrical And Photoluminescence Measurements.

BPR / T_s	2:1	1:1	1/2:1	1/4:1
250		μ_p=1490 N_D=9.5x10^{16} N_A=8.0x10^{16} η_{300}=1.4x10^{16} ρ_{300}=1.5 R=29 I_X=3.6x10^4 ΔE=3.75		
300		μ_p=2400 N_D=8.2x10^{16} N_A=3.7x10^{16} η_{300}=4.0x10^{16} ρ_{300}=0.42 R=500 I_X=1.0x10^5 ΔE=2.0	μ_p=2130 N_D=1.7x10^{17} N_A=1.1x10^{17} η_{300}=4.9x10^{16} ρ_{300}=0.30 R=1100 I_X=2.0x10^5 ΔE=2.25	
350		μ_p=5650 N_D=3.3x10^{16} N_A=2.3x 10^{16} η_{300}=9.4x10^{15} ρ_{300}=1.5 R=830 I_X=1.0x10^5 ΔE=1.6	μ_p=3750 N_D=5.8x10^{16} N_A=4.2x10^{16} η_{300}=1.5x10^{16} ρ_{300}=1.1 R=700 I_X=1.0x10^5 ΔE=2.0	μ_p=2350 N_D=8.9x10^{16} N_A=7.4x10^{16} η_{300}=1.3x10^{16} ρ_{300}=1.2 R=300 I_X=3.7x10^4 ΔE=2.5
400		Very resistive $\rho_{300} \geq 250$ R=13 I_X=7500 ΔE=2.6	μ_p~1700 Very resistive ρ_{300}~100 R=40 I_X=2.0x10^4 ΔE=2.0	Highest ρ to date ρ_{300}~10,000 R=8 I_X=1500 ΔE=3.75

(a)

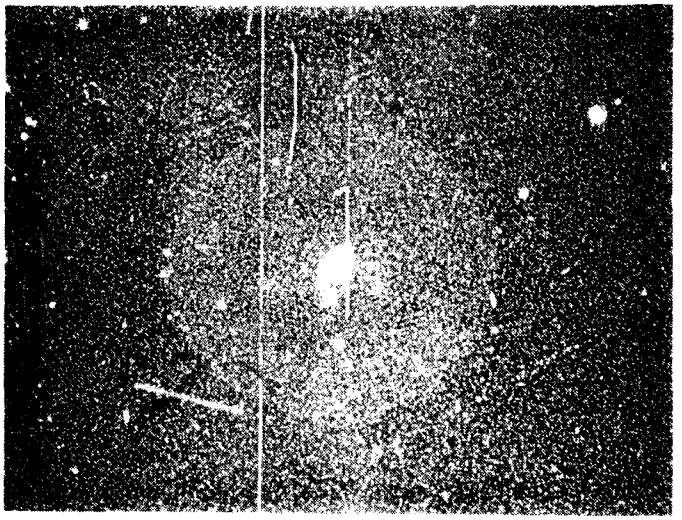

(b)

Figure 2-1. Micrographs Of ZnSe Surface On First Exposure To Room Ambient (a), And After Three Months (b).

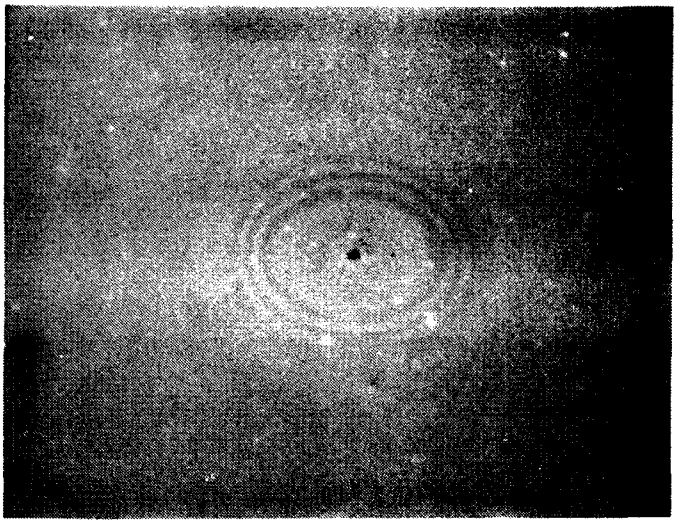

(a)

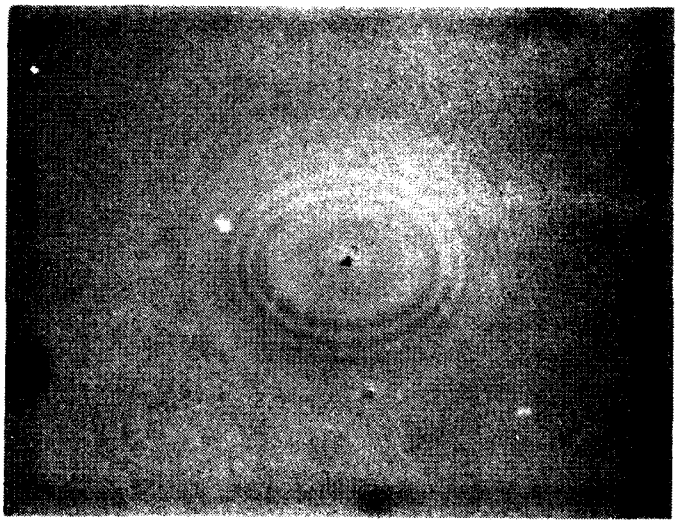

(b)

Figure 2-2. Interference Contrast Micrographs Reveal No Changes From Pristine Sample (a) And After Two Months Exposure To Room Ambient (b).

system from exposure to atmosphere. Samples ZSE30-ZSE33 show a monotonic "clean-up" of the system: PL spectra (Figure 2-3) shows the donor-bound excition (DBE) line in the band edge emission narrowing dramatically and shifting to higher energy with subsequent growth runs. There is a corresponding increase in the R-value and a decrease in the relative contribution of the Cu-green band (2.5eV) to the deep level (DL) emission. We have concluded that, after exposure to atmosphere for source replenishment, the MBE system requires the equivalent of 3-4 growth runs to clean up surface contaminants before high quality layers can again be grown. Samples in the subsequent series, ZSE33-ZSE35, grown under identical conditions, show no discernible difference in their PL, indicating excellent run-to-run and day-to-day reproducibility in our growth process.

Samples in the series ZSE37-ZSE46 are part of the 16-sample series designed to explore the BPR-T_s growth parameter space. As can be seen in Table 2-1, we have found a reasonably good correlation between the PL and electrical measurements on these samples. Good electrical properties (high mobility, low donor and acceptor concentrations) have been demonstrated in those films which show the best PL results (large R-value and donor-bound exciton emission intensity, and small donor-bound exciton linewidth). At this stage, it appears that the optimum growth parameters are going to fall in the vicinity of T_s=300-350°C and BPR=1.0-0.5.

Our paper entitled "Effects of Strain on the Energy Band Gap in Heteroepitaxially Grown ZnSe" was prepared and submitted for publication. The major quantitative results of this study are summarized in Figure 2-4 where we show the shift in the ZnSe bandgap, as determined by shifts in the dominant DBE peak in PL, plotted vs. strain, as derived from published X-ray measurements of the lattice parameter of ZnSe on GaAs vs. film thickness. Here we see a variation of E_g which approximates that predicted [see the E_o (1) curve in Figure 2-4] using bulk lattice parameters. More important than this quantitative result, which is quite a crude estimate given in view of the several approximations made, is the qualitative demonstration that E_g increases with increasing biaxial compression, in agreement with the published behavior of several III-V zincblende semiconductor systems, but in contrast to the behavior predicted for ZnSe by some authors.

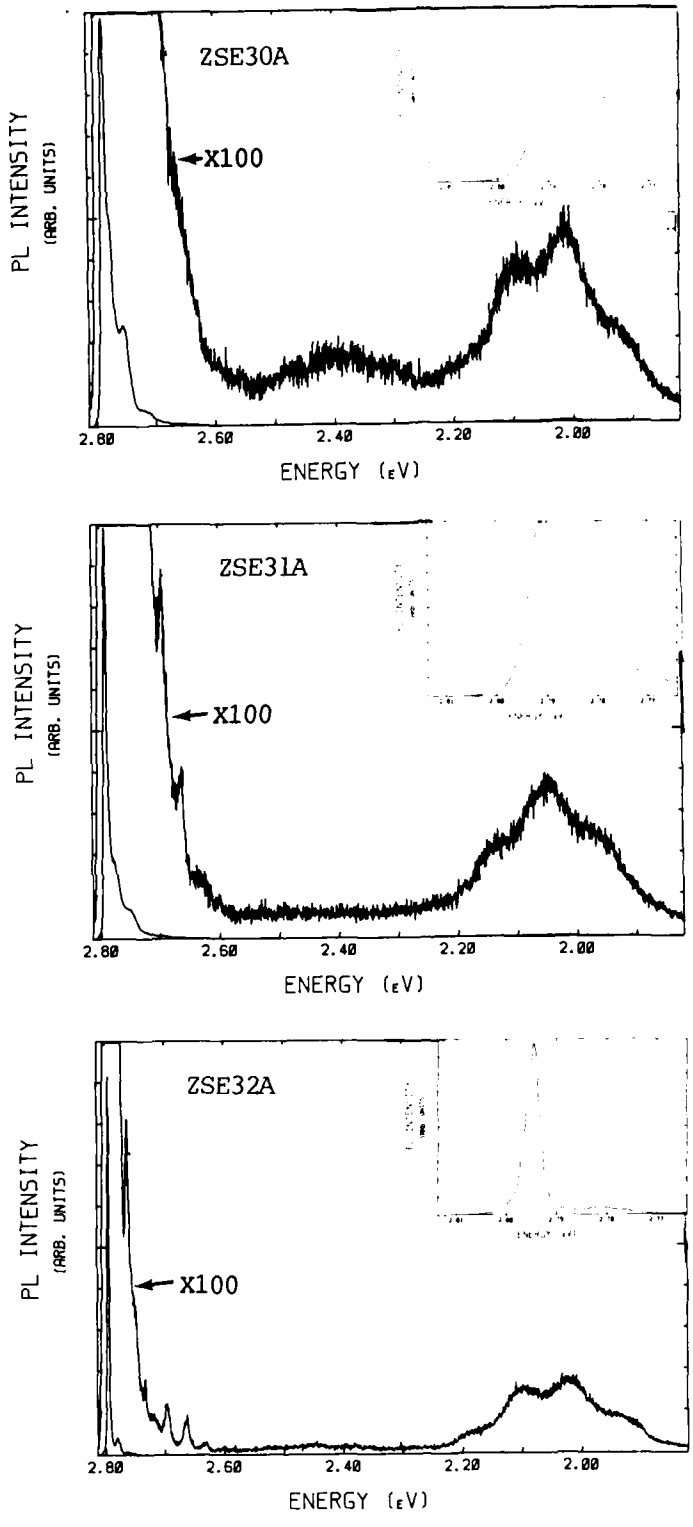

Figure 2-3. Low-Temperature PL Spectra Of Three Layers Grown Immediately After Reloading Sources.

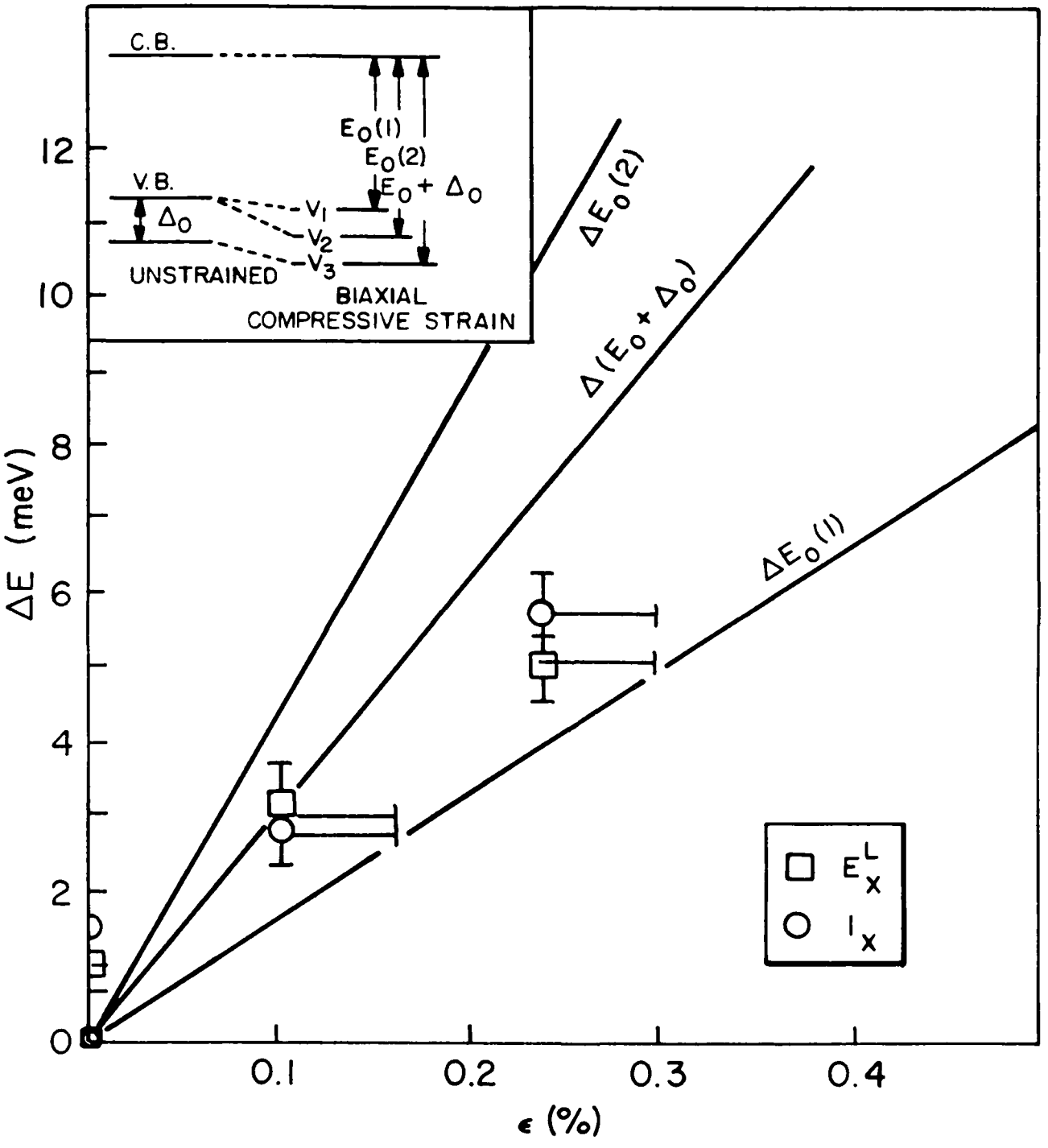

Figure 2-4. Shift In The Donor-Bound Exciton And Free Exciton PL Peak Position With Strain In ZnSe.

A new dye laser and its large-frame Ar-ion laser pump have been installed for use in performing selective excitation photoluminescence (SEPL) measurements. A continuous-flow liquid helium cryostat has also been installed to replace our closed-cycle refrigerator when performing SEPL measurements at T=4.2K. These changes have necessitated a complete revamping of our input and collection optics systems; this restructuring of the system is now nearly completed. In the course of testing and calibrating the dye laser system, we have performed some preliminary SEPL measurements on one of our recent MBE ZnSe films (ZSE37A); representative spectra are seen in Figure 2-5. In (a) we show the NBE emission obtained under normal (i.e., non-resonant) excitation conditions. Note the clear resolution of the donor-bound exciton "peak" into two components, centered at 22561cm^{-1} (2.7965eV) and 22545cm^{-1} (2.7945eV); also note the weak and relatively unstructured emission in the vicinity of 22450cm^{-1} (2.775eV). The arrows in Figure 2-5(a) show the positions of the laser excitation for subsequent scans. Figure 2-5(b) through (d) demonstrate the strong enhancement of the emission in the 2.777eV region when using resonant excitation, and they show the strong variations in spectral structure obtained in this region as the laser is tuned through the various components of the donor-bound exciton "peak". Much more detailed and careful measurements must be performed before any meaningful analysis can be attempted. This study will begin during the next quarter; we anticipate that this tool will give us valuable information to correlate with our SIMS measurements in our efforts to identify the relevant donor species in the ZnSe films.

2.1.1.3 Dependence of Electrical Characteristics Upon Growth Conditions

In this section we describe the results of Hall measurements on the ZnSe/GaAs series (ZSE37A - ZSE46A). In this study we observed:

(a) electron mobilities greater than 5600 cm^2/volt-sec,

(b) donor densities, N_D, less than $4 \times 10^{16} cm^{-3}$, and

(c) room temperature carrier concentrations, n_{300}, less than $1 \times 10^{16} cm^{-3}$.

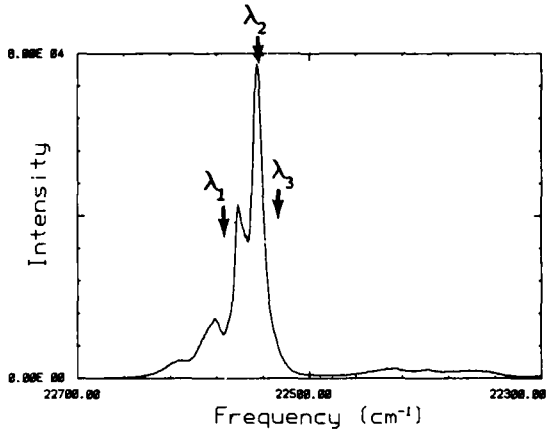

(a)

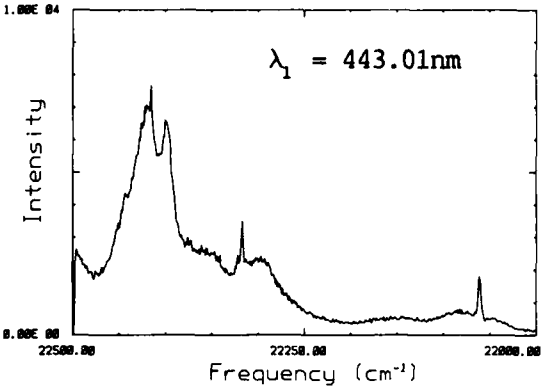

(b)

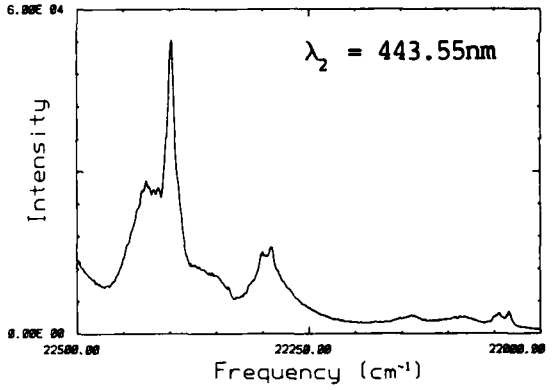

(c)

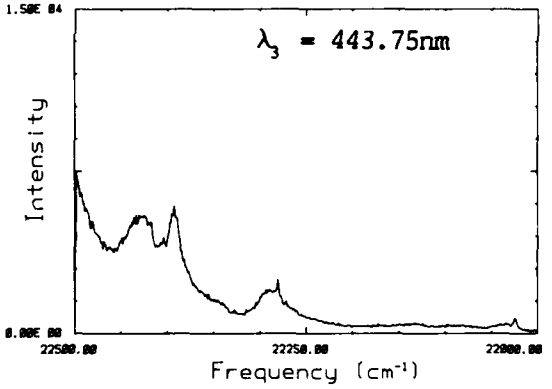

(d)

Figure 2-5. Selective Excitation PL Spectra (b-d) And For Excitation Energies Indicated In (a).

Hall measurements were made at temperatures from 17K to 300K utilizing the van der Pauw technique. The magnitude of the applied magnetic field was 2.0 Tesla and the currents were 1μA to 20μA. The carrier concentration, n, and mobility, μ, versus temperature, are shown in Figures 2-6 and 2-7.

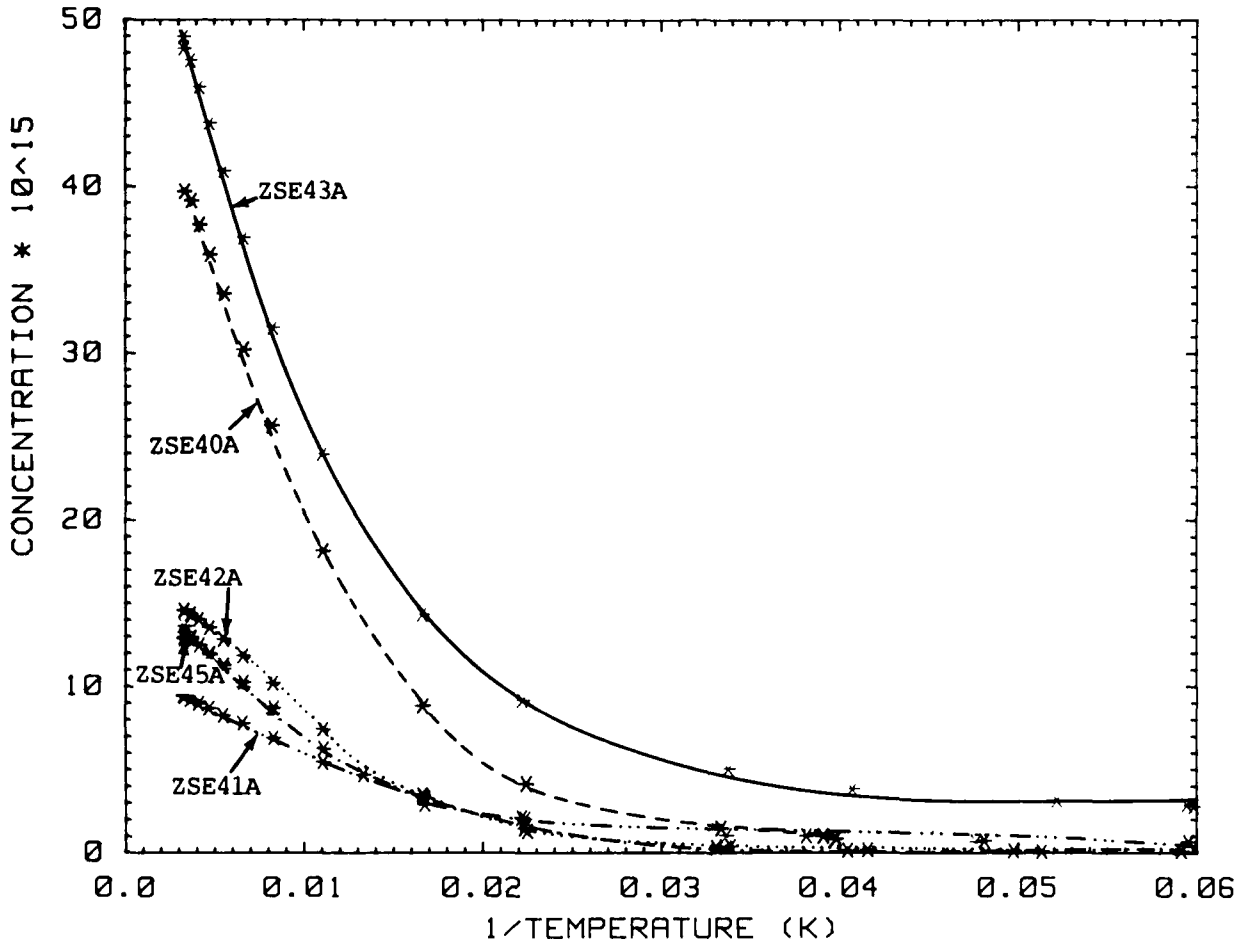

Figure 2-6. Carrier Concentration Versus Reciprocal Temperature In Kelvin.

The donor density, N_D, acceptor density, N_A, and donor ionization energy, E_D; were determined by fitting the carrier concentration to:

$$\frac{n\,(n + N_A)}{N_D - N_A - n} = \left(\frac{N_c}{g}\right) \exp\left(-\frac{E_d}{kT}\right)$$

Where $N_C = 2\left(\frac{2\Pi m_e^* kT}{h^2}\right)^{3/2}$ and g=2.

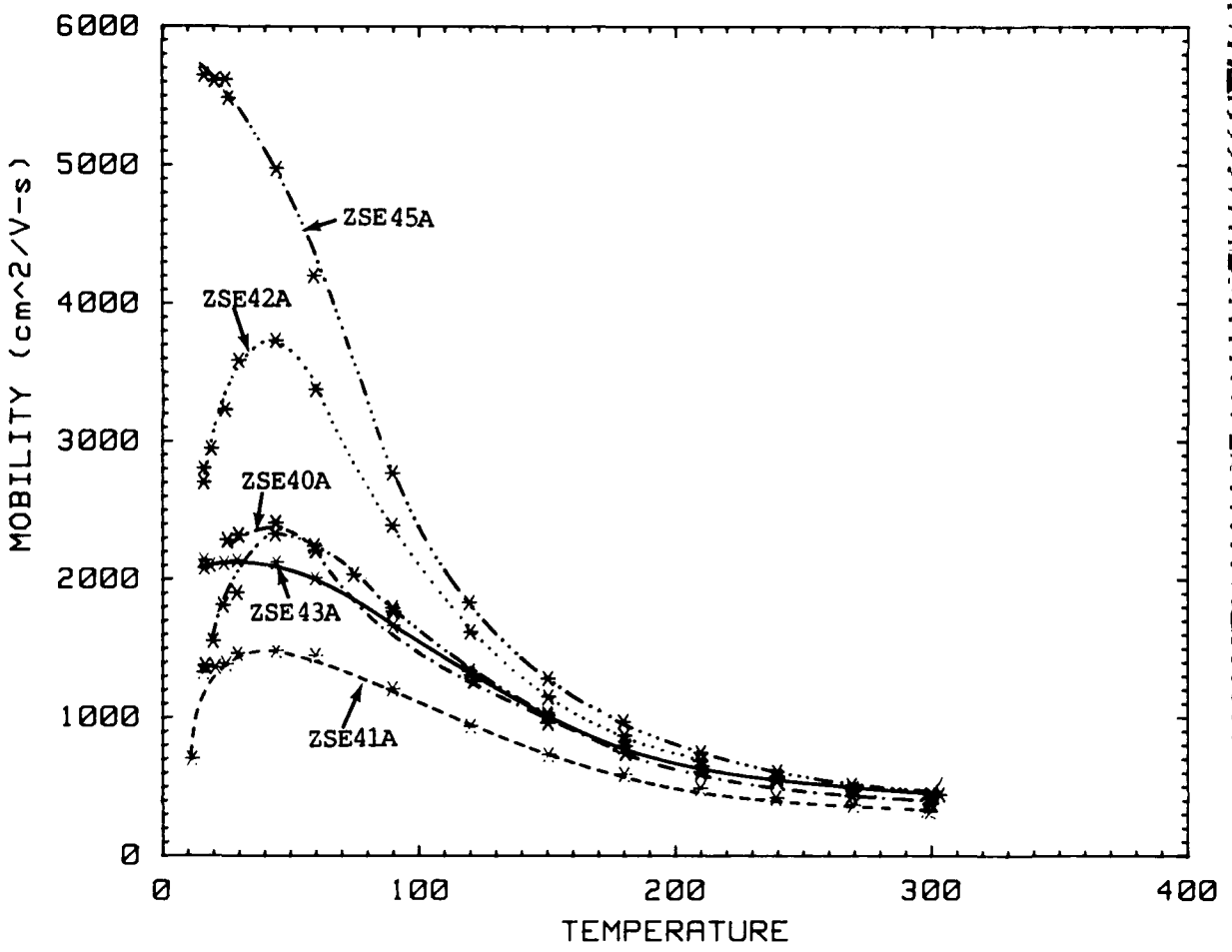

Figure 2-7. Electron Mobility Versus Temperature In Kelvin.

and m_e^* is the effective mass of the carriers (electrons), h is Planck's constant and k is Boltzmann's constant. The results for N_D and N_A are displayed in Table 2-1 along with the peak mobilities, room temperature carrier concentrations and room temperature resistivities.

The four samples which were grown at 400°C (ZSE38A, ZSE39A, ZSE44A, and ZSE46A) were of very high resistivity and for all but ZSE39A, Hall mobility measurements could not be made. Preliminary measurements on ZSE39A indicate a peak mobility of approximately 1700cm^2/volt-sec and a room temperature carrier concentration of 4 x $10^{14}cm^{-3}$. The Hall mobility is determined

predominantly by polar optical phonon and ionized impurity scattering. Since polar optical phonon scattering is nearly sample independent, a small peak mobility indicates a large concentration of donors and acceptors. The low carrier concentration along with the low peak mobility observed in ZSE39A, therefore, indicates large compensation, that is large N_A+N_D and small N_D-N_A.

If the ionized impurity concentration, $N_I=N_A+N_D$, is taken as a measure of film quality, then the optimum growth conditions thus far encountered are $T_s=350^\circ C$ and BPR=1:1 where T_s is the growth temperature and BPR is the zinc to selenium beam pressure ratio. N_I was observed to increase as the growth temperature was reduced from $350^\circ C$ while holding the beam pressure ratio contant. As mentioned previously, the concentration of ionized impurities also appeared to increase as the growth temperature was raised above $350^\circ C$. For fixed temperature, N_I was found to increase as the Zn to Se BPR was reduced from 1:1. The effect of increasing the Zn to Se pressure ratio will soon be examined.

2.1.1.4 MBE Relaxation and Reproducibility of Growth Conditions

As mentioned in Section 2:1.1.1 (B), layers ZSE30A-ZSE32A were grown to investigate the "recovery" of the MBE system after reloading the source material, and ZSE33A-ZSE35A were grown to investigate sample reproducibility. As can be seen in Table 2-2, the room temperature carrier concentrations decreased and the peak mobilities increased from ZSE30A to ZSE32A. This strong improvement in film quality indicates the need for the MBE system to "recover" after reloading source material, or the need to thoroughly outgas the source material prior to growth.

Run-to-run reproducibility was investigated with the growth of ZSE33A-ZSE35A. All three films were grown under the same nominal conditions on different days. Figures 2-8 and 2-9 show the temperature dependence of the carrier concentrations and mobilities for the three samples. The electrical characteristics of ZSE33A-ZSE35A are seen to be very similar and confirm our ability to reproduce the growth conditions.

TABLE 2-2. Room Temperature Carrier Concentrations And Peak Mobilities For ZSE30A To ZSE35A

SAMPLE NUMBER	η_{300} ($x10^{16}$ cm^3)	μ_p (cm^2/Volt-sec)
ZSE30A	15.1	550
ZSE31A	9.9	800
ZSE32A	8.6	1220
ZSE33A	7.2	1100
ZSE34A	8.3	1160
ZSE35A	8.6	1090

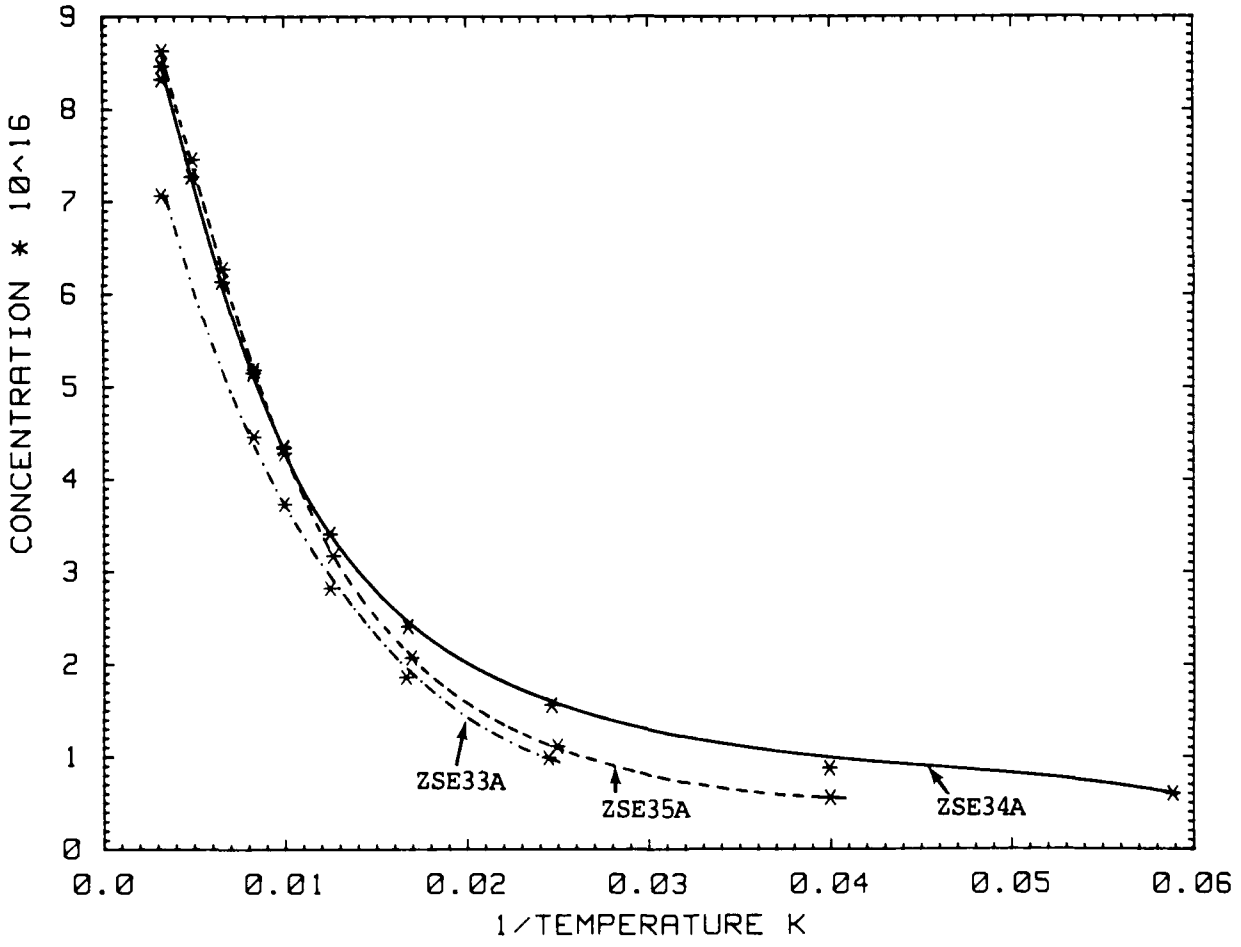

Figure 2-8. Carrier Concentration Versus Reciprocal Temperature For ZSE33A To ZSE35A.

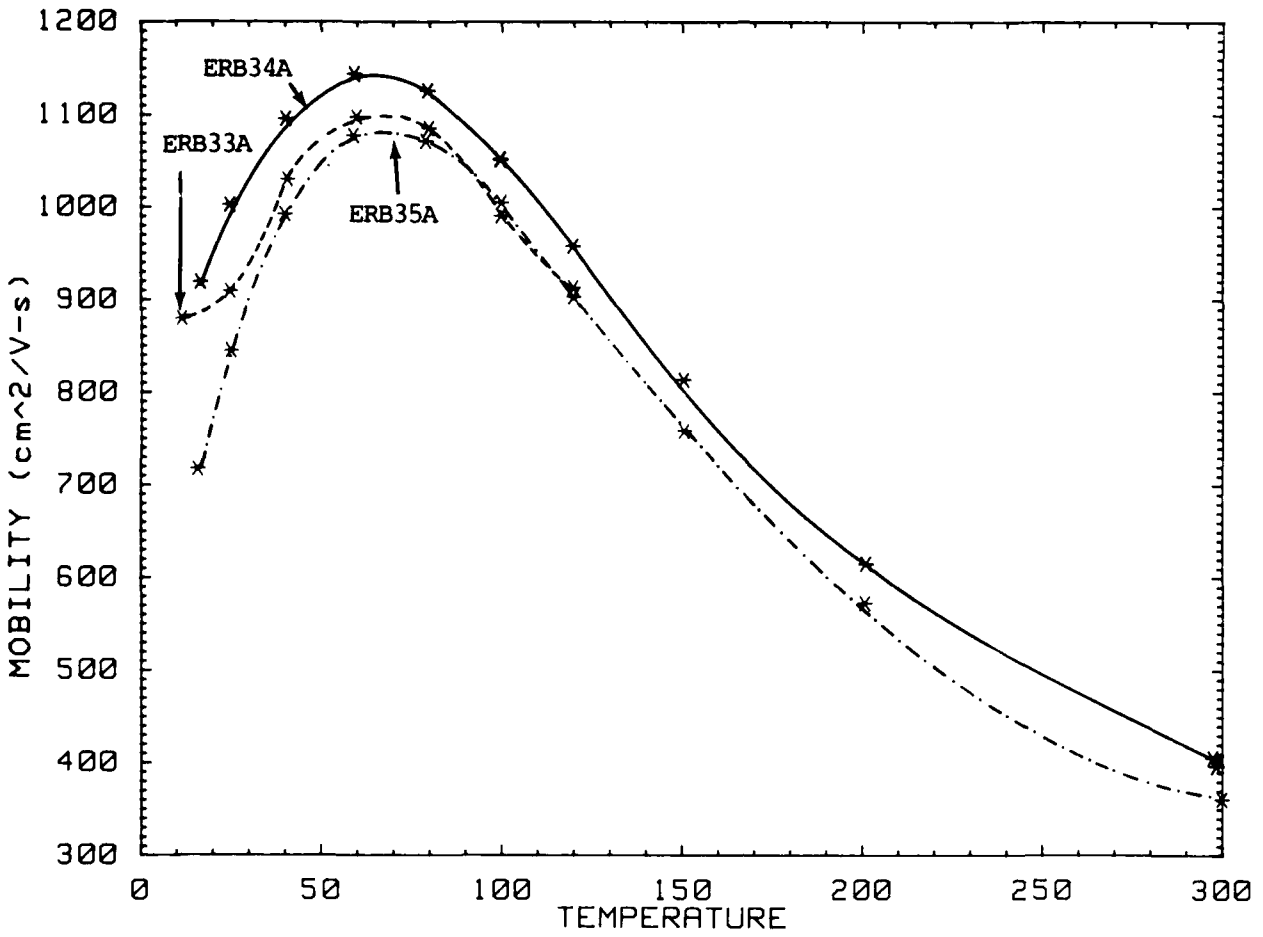

Figure 2-9. Electron Mobility As A Function Of Temperature For ZSE33A to ZSE35A.

2.1.2 ZnSe Heteroepitaxy on (100)Ge Buffer Layers

It is well known in the literature that the properties of an epitaxial layer are profoundly influenced by the physical and chemical characteristics of the substrate surface from which growth proceeds. Thus, damage to the surface incurred during cleaning or failure to thoroughly remove impurity atoms adsorbed on the substrate surface generally results in layers of poor quality. As described in Six Month Technical Progress Report No. 1, the preferred cleaning technique for the (100)Ge substrate is room temperature sputtering and a subsequent anneal at about 400°C prior to growth of the epitaxial layer [1]. The thermal desorption technique was found to result in ZnSe layers of poor quality as measured by RHEED and photoluminescence

(PL). Nonetheless, the sputter/anneal technique leaves a surface that is relatively rough as indicated by RHEED and, by its nature, introduces many sub-surface defects into the substrate. In an attempt to alleviate the problem of substrate defect replication in the ZnSe epitaxial layer, and to provide an atomically smooth surface on which to initiate growth, a Ge buffer layer was deposited on the sputter/annealed surface prior to growth of the ZnSe epitaxial layer.

In this section, the MBE growth of unintentionally doped ZnSe on (100)Ge substrates with a Ge epitaxial buffer layer is reported, the low-temperature PL measurements of the ZnSe epitaxial layers are presented, and the results discussed. In addition, a brief study of ZnSe grown on a Ge buffer layer on a (100)Si substrate is reported.

2.1.2.1 Growth Conditions for ZnSe Epitaxial Layers on (100)Ge with a Ge Buffer Layer

Homoepitaxial Ge buffer layers were grown on (100)Ge substrates prepared for growth as described in Section 2.1.2 in Six Month Technical Progress Report No. 1. Ge was evaporated from source material in a Knudsen cell installed on the MBE growth chamber. Prior to loading with Ge, the K-cell with a PBN crucible was outgassed in the chamber at a temperature of 1350°C for several hours. The crucible was then charged with 6N's Ge material and the K-cell outgassed at 1300°C. The Ge flux calibration is shown in Figure 2-10, which is a plot of Ge beam pressure monitored at the substrate location versus reciprocal K-cell temperature. Useful Ge fluxes are obtained at K-cell temperatures above 1250°C. A beam pressure of 4×10^{-7} mbar was found to correspond to a Ge epitaxial layer growth rate of about 0.1 μm/h. The substrate temperature selected for the Ge buffer was 330°C which is near the "optimum" growth temperature for ZnSe on the sputter/annealed (100)Ge substrate, and the growth rate used was 0.1 μm/h. Figure 2-11(a) and (b) show RHEED patterns recorded from a sputtered and annealed (100)Ge substrate and a Ge epitaxial layer, respectively. In both cases the surface reconstruction was (2x2). However, on initiating growth of the Ge layer, the streaks became more intense and sharp and the Kikuchi band became better defined.

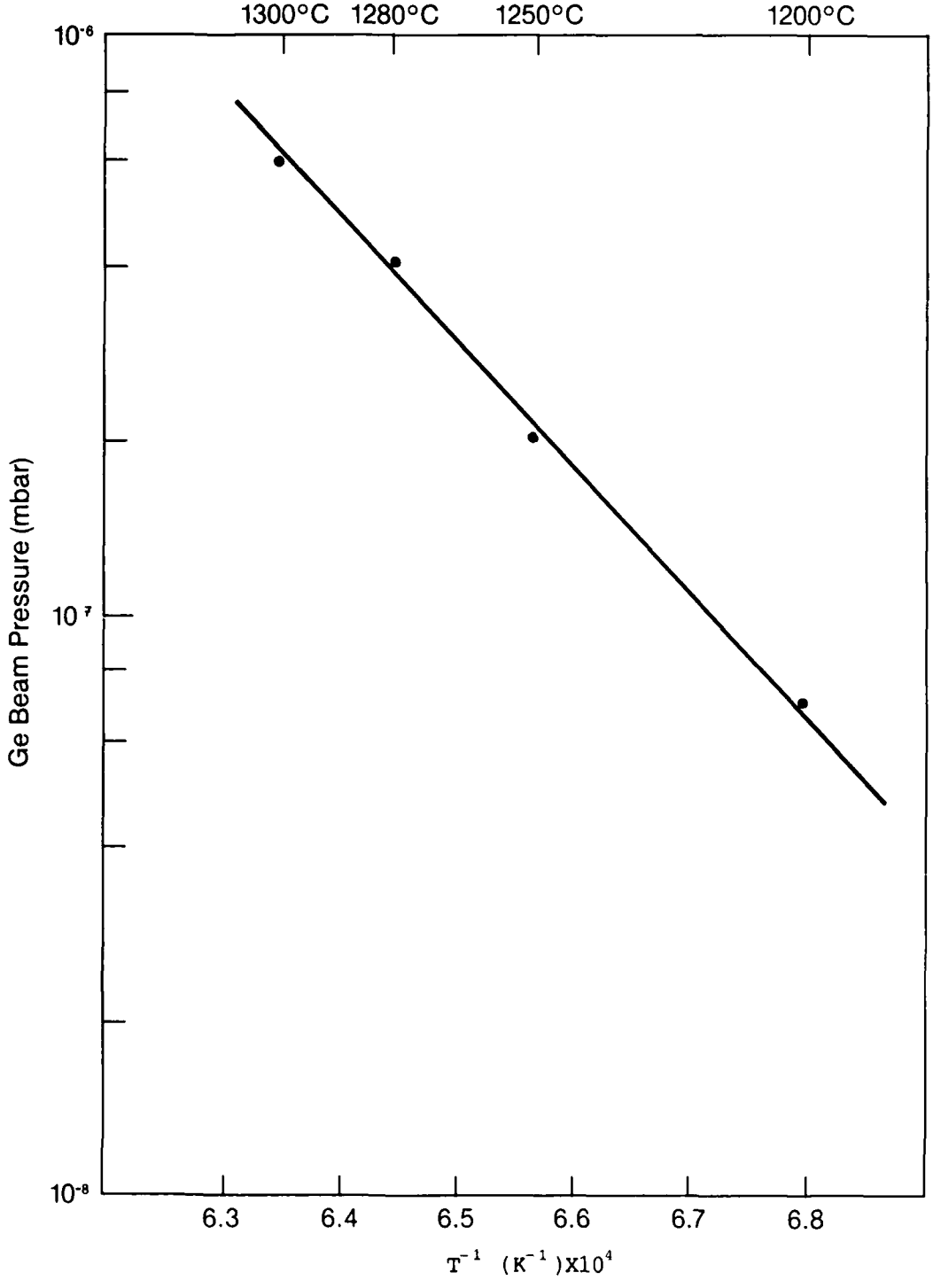

Figure 2-10. Ge Beam Pressure Monitored At The Substrate Location Versus Reciprocal K-Cell Temperature.

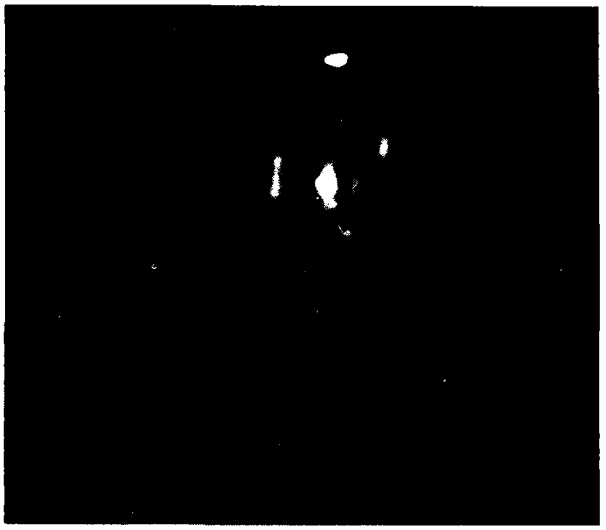

(a)

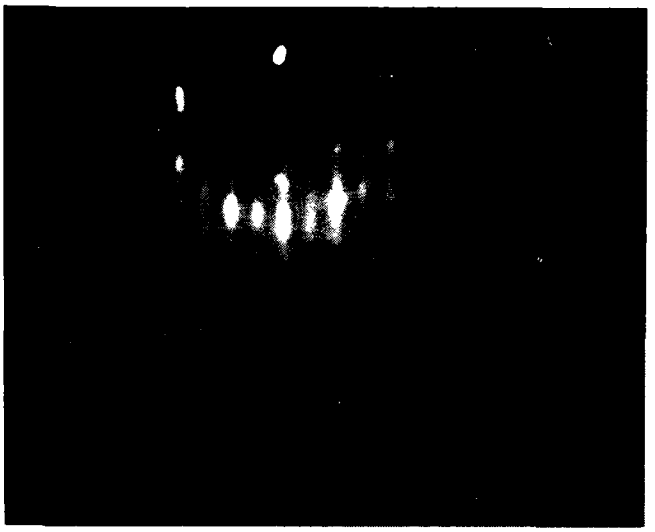

(b)

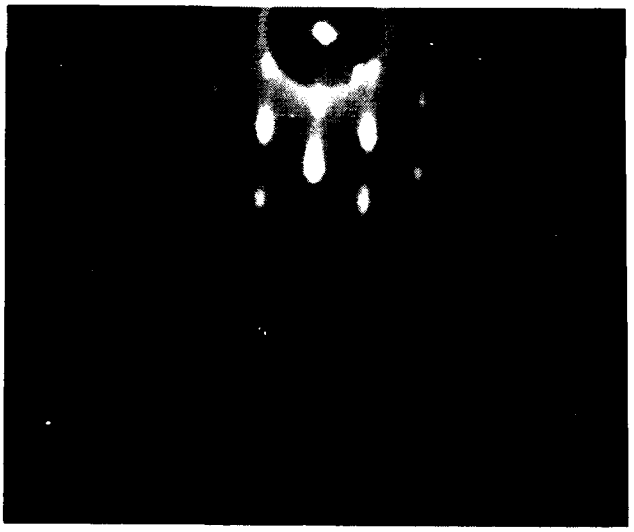

(c)

(d)

Figure 2-11. RHEED Patterns Of (a) The Sputter/Annealed Ge Substrate, (b) Ge Epitaxial Layer, (c) 2 μm Thick ZnSe On A Ge Substrate, and (d) ZnSe On A 1000 Å Thick Ge Buffer Layer.

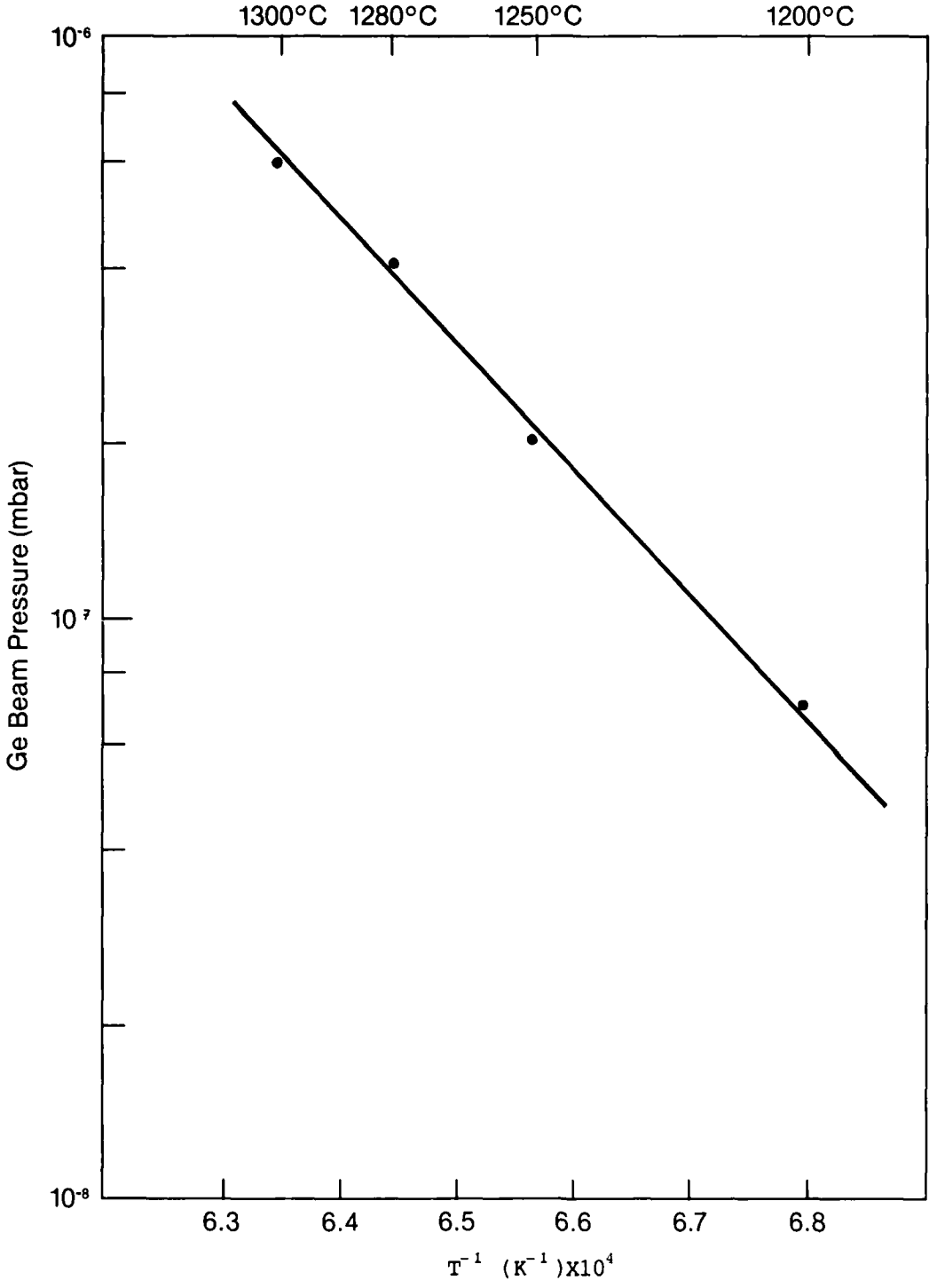

Figure 2-10. Ge Beam Pressure Monitored At The Substrate Location Versus Reciprocal K-Cell Temperature.

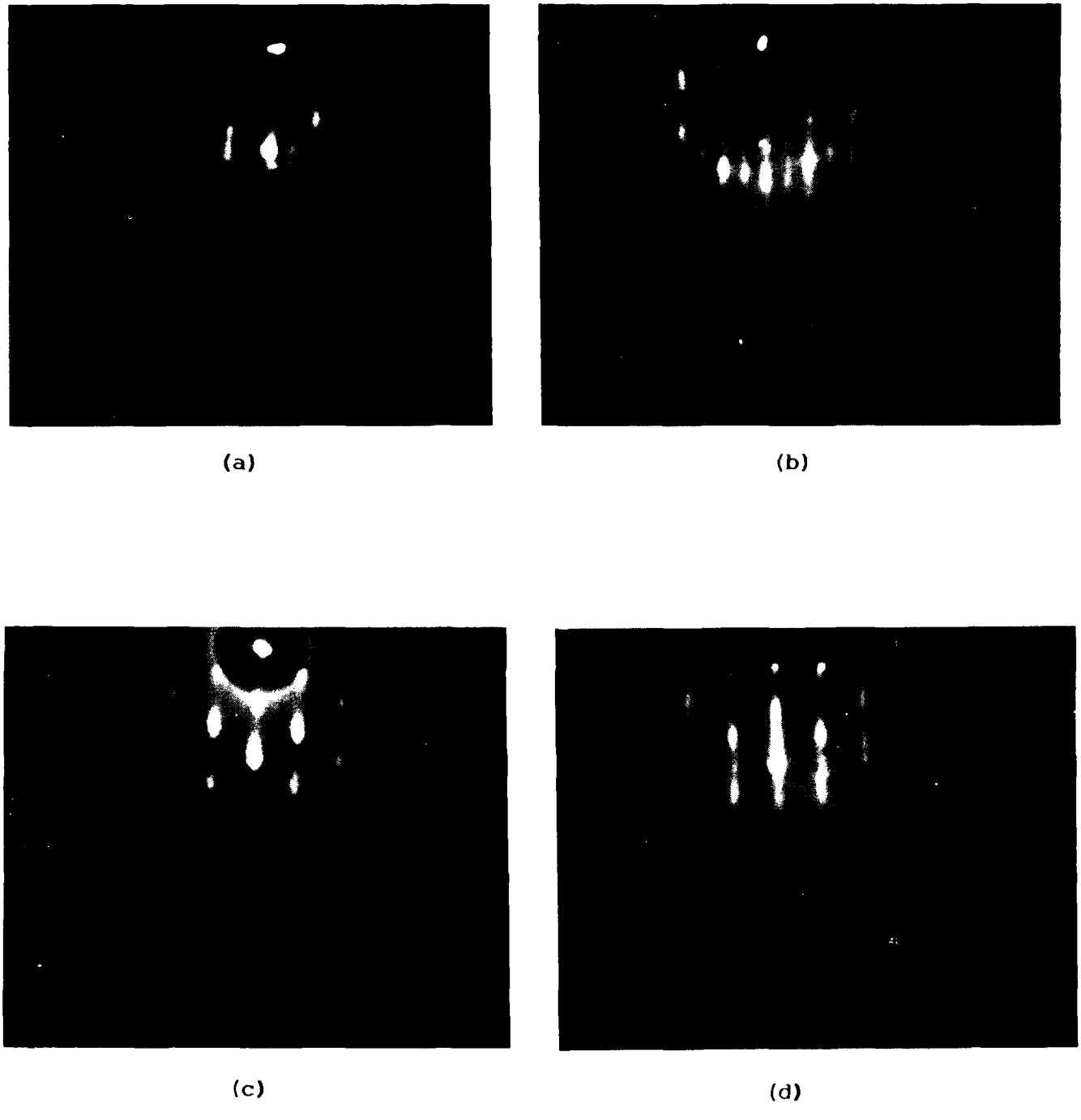

Figure 2-11. RHEED Patterns Of (a) The Sputter/Annealed Ge Substrate, (b) Ge Epitaxial Layer, (c) 2 μm Thick ZnSe On A Ge Substrate, and (d) ZnSe On A 1000 Å Thick Ge Buffer Layer.

ZnSe layers have been grown on Ge epitaxial layer buffers with thicknesses from 200A to 2μm; the results of low-temperature PL measurements will be reported below. Figure 2-11(c) and (d) show RHEED patterns recorded from 2μm thick ZnSe layers grown without a Ge buffer and with a 1000A thick Ge buffer, respectively. It is evident from the RHEED patterns that the ZnSe layer is smoother on an atomic scale when growth is initiated on a Ge buffer. The growth temperature for both the Ge and ZnSe layers was 330°C. All ZnSe layers were 2μm thick.

2.1.2.2 Growth of ZnSe Epitaxial Layers on (100)Si with a Ge Buffer

We reported in the literature the growth of single crystal ZnSe layers on (100)Si [2]. It was found that single crystal ZnSe is obtained provided the growth rate of the ZnSe layer is initially very slow; if the growth is initiated at a high rate, poly-crystalline ZnSe is invariably obtained. It was therefore decided to do a brief study on the growth of ZnSe on a (100)Si substrate using a Ge buffer.

Figure 2-12(a) shows the RHEED pattern of the cleaned Si substrate, and it is seen to exhibit a (2x1) reconstructed surface. On initiation of growth of the Ge buffer, the (2x1) pattern gives way to a Ge (2x2) superstructure shown in Figure 2-12(b). The ZnSe RHEED pattern shown in Figure 2-12(c) is indicative of a rough surface on an atomic scale. This pattern is quite similar to that obtained from a ZnSe layer grown directly on Si. However, the important point to note here is that unlike growth without a Ge buffer, ZnSe growth can be initiated directly at a high rate.

2.1.2.3 Photoluminescence Measurements on ZnSe Layers Grown on (100)Ge Buffer Layers

ZnSe epitaxial layers grown on (100)Ge substrates with Ge homoepitaxially grown buffer layers from 200A to 2μm thick as described above were studied by the low-temperature PL technique. Measurements of the 4.2K PL spectra were taken using the 365nm line of a Hg(Xe) lamp as the source of excitation and with an excitation intensity of about 50mW/cm^2. Figure 2-13(a) shows the emission spectrum of a ZnSe layer grown on (100)Ge

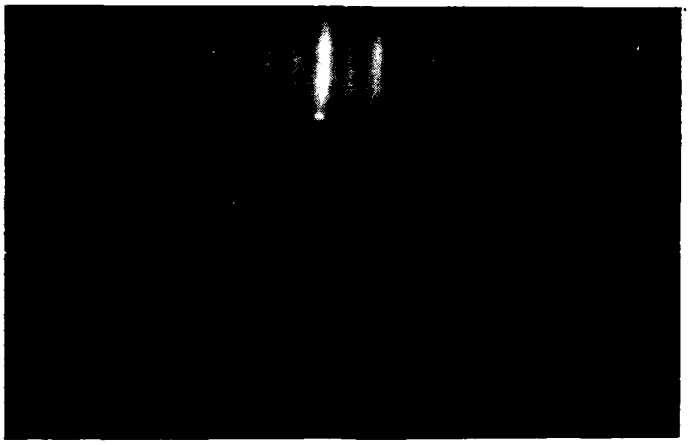

(a)

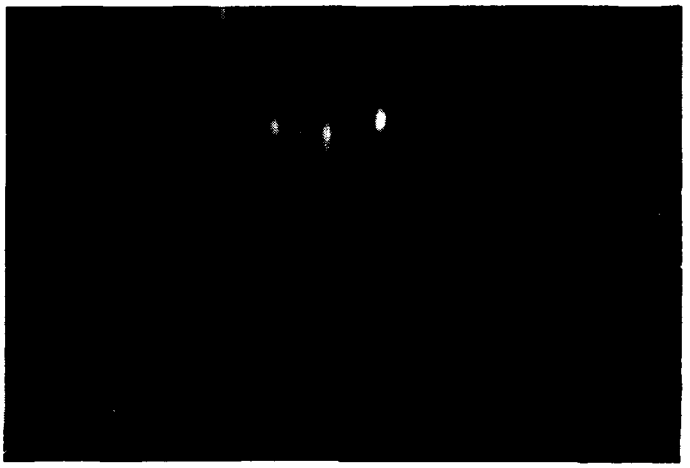

(b)

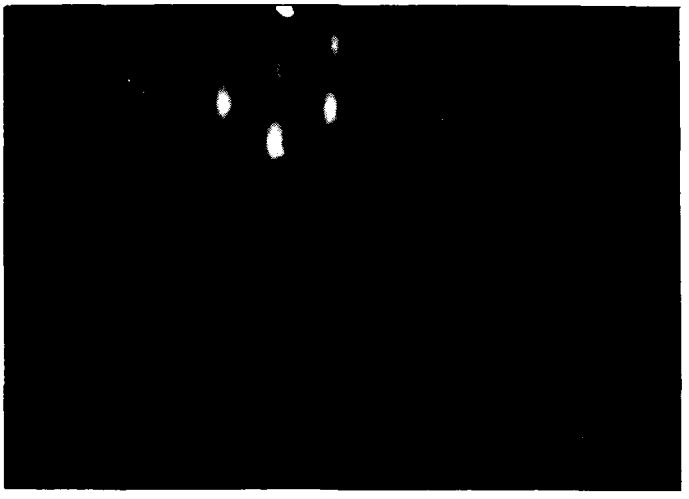

(c)

Figure 2-12. RHEED Pattern Of (a) The Sputter/Annealed (100) Si Substrate. The Streaky RHEED Pattern Of The Ge Epitaxial Layer (b), Gives Way To A Spotty Pattern Of The ZnSe (c).

with a 0.625 μm thick Ge buffer. The emission is dominated by near band-edge emission line at 2.7978eV and a relatively broad band with peaks resolved at 2.8007eV, 2.8018eV, and 2.8038eV, probably due to free exciton (FE) emission and shown in greater detail in the inset. Note that the FWHM of the I_2 peak is a remarkable 0.87meV. Notice too the shoulders at about 442.9nm, and at 443.2nm and 443.5nm on the low energy skirt of I_2. Figure 2-13(b) shows the prominent I_1^{deep} emission line which is very narrow (FWHM about 1.4meV) and which has been associated with a bound exciton either at an intrinsic defect or a substitutional Cu impurity, as well as the I_1 peak at 2.777eV. LO-phonon replicas of these peaks are quite evident and well resolved. By comparison, the 4.2K PL spectrum of ZnSe grown on (100)Ge without a buffer [Figure 2-13(c)] reveals relatively weak near band-edge emission; the deep-level emission from 550nm to 620nm remained essentially constant irrespective of Ge buffer layer thickness. The dominant emission line is I_2, located at 2.7976eV with a linewidth of about 2.1 meV (see inset). The weak FE band peaks at about 2.8018eV. It is interesting to note that I_1^{deep} , which is prominent in the PL spectrum of ZnSe grown on the 0.625 μm buffer, is not evident in that of ZnSe grown without a Ge buffer. In fact, from Figure 2-14(a), there is an apparent monotonic increase in the amplitude of I_1^{deep} to a buffer thickness of about 0.63 μm and, beyond that, there is a small decrease. Similarly, from the figure, there is an apparent maximum in the amplitude of the I_2 emission and a corresponding decrease in its linewidth [shown in Figure 2-14(b)]. Since the ZnSe epitaxial layers have nominally the same thickness and the growth conditions are the same, the increase in the amplitude of I_1^{deep} with buffer layer thickness is interesting. However, without data from other characterization techniques, we can only speculate on the cause. We have plans to do high resolution TEM and double-crystal X-ray diffractometer measurements on these layers during the next three months. It is also interesting to note that the I_2 peak amplitude increases by almost two orders of magnitude as the buffer layer thickness is increased to 0.625 μm. Nonetheless, the very narrow linewidths of the shallow I_2 peak (FWHM~0.87meV) and the deeper I_1^{deep} peak (FWHM~1.4meV) suggest that in the volume sampled by PL, the ZnSe is of very high crystallographic quality.

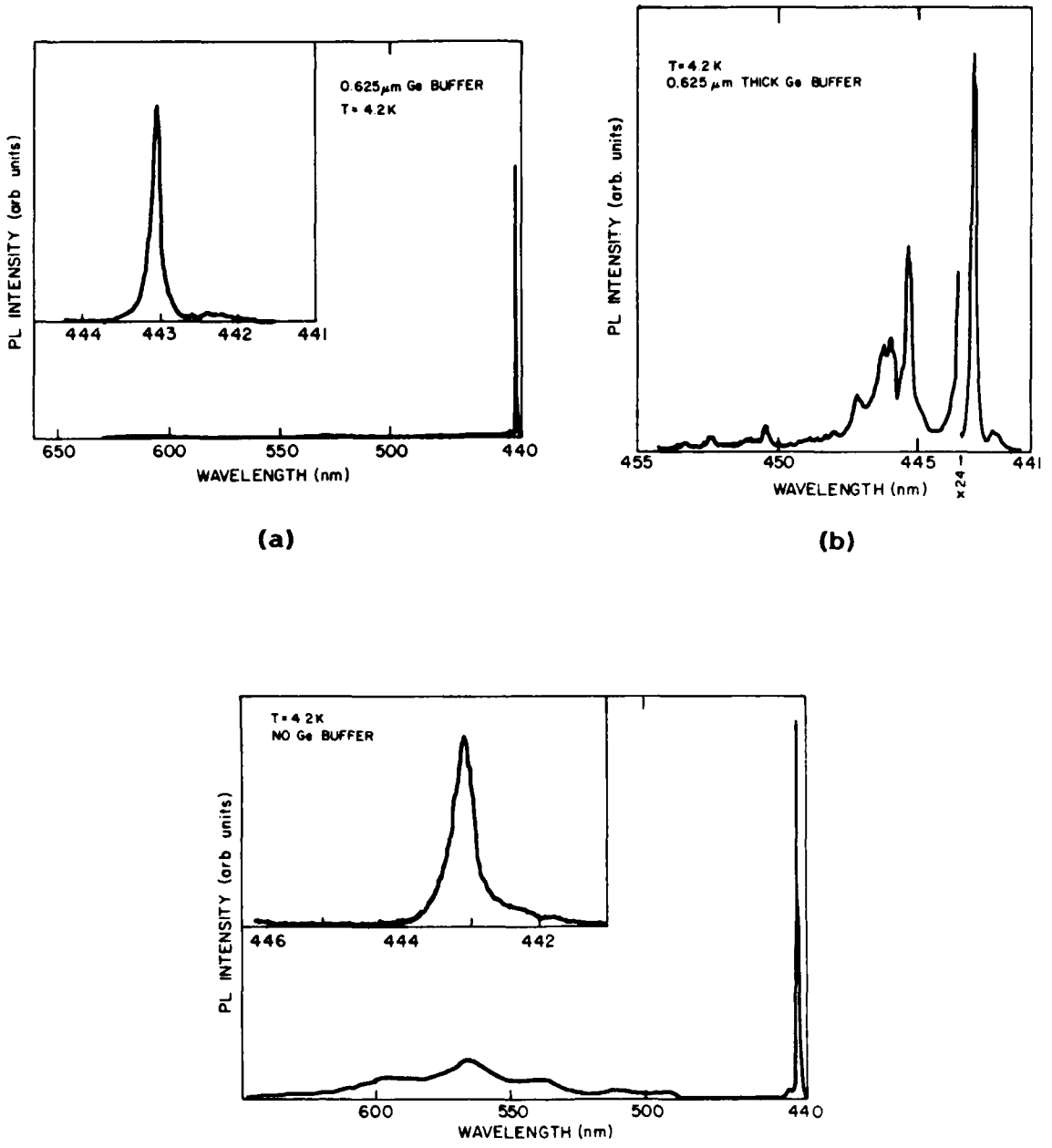

Figure 2-13. (a) Low-Temperature PL Spectrum Of ZnSe Grown On (100) Ge with A 0.625 μm Thick Ge Buffer Is Shown In Greater Detail In (b). (c) PL Spectrum Of ZnSe/(100)Ge without A Ge Buffer.

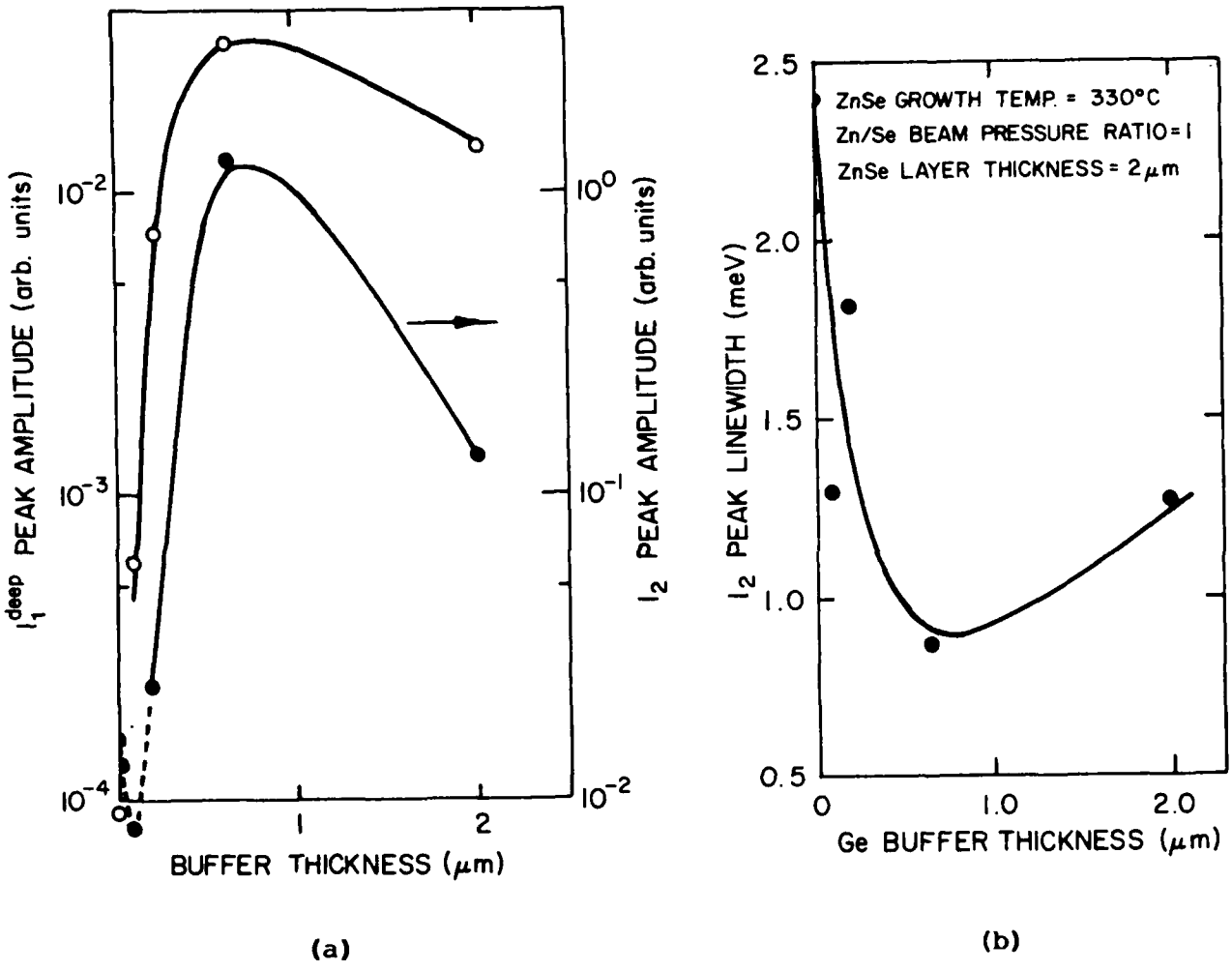

Figure 2-14. (a) I_1^{deep} And I_2 Peak Amplitudes Of ZnSe Grown On (100) Ge Buffers Versus Buffer Thickness. The Corresponding Linewidth Of I_2 Is Shown In (b).

2.1.3 ZnSe Heteroepitaxy on (211)Ge

The growth of GaAs on (100)Si is similar to that of ZnSe on (100)Si to the extent that the lattice mismatch is similar in both cases as well as the fact that one is growing a polar material on a non-polar substrate. In the case of epitaxial growth of a polar material on a non-polar substrate, anti-phase domains (APD) are formed and their effects on the electrical and optical characteristics of the layers are important considerations. Various approaches have been used to reduce, if not eliminate, APD formation. One approach which apparently has been successful in the epitaxial growth of GaAs on Si is the use of a (211)Si substrate. The reasons for the success are not yet clear. Nonetheless, a preliminary study on the epitaxial growth of ZnSe on (211)Ge seems worthwhile. To date only one layer has been grown and characterized by low-temperature PL. However, the results are interesting enough to be included in this report.

2.1.3.1 Growth and Characterization of ZnSe on (211)Ge

The cleaning technique used to prepare the (211)Ge for epitaxial growth was identical to that used for preparing the (100)Ge substrates, and the growth conditions were identical to those used for growth of "optimum" ZnSe on (100)Ge, namely, a Zn to Se beam pressure ratio of approximately 1 and a substrate temperature of about 330°C. The 4.2K PL spectrum of the layer shown in Figure 2-15(a) exhibits the usual features, namely, S-A emission at about 615nm, a green emission band at about 540nm, and the S series of peaks (also referred to as the M band) at about 500nm. However, the fact that the emission is dominated by a very narrow emission line (probably I_1^{deep}) at about 445nm is unusual. Figure 2-15(b) shows this emission band in greater detail. The peak energy is 2.7837eV (445.28nm) with three phonon replicas as indicated on the figure. The FWHM of the no-phonon line is about 1.3meV which is comparable with that of the shallower DBE lines of our better-quality layers. The intensity of this emission is greater than that of any layer we have observed to date on any substrate used in this study. However, the amplitude of the I_2 peak at 2.798eV (443nm) is comparable with that of layers grown on (100)Ge without and with a Ge buffer. The shoulder on the low-energy skirt of the no-phonon peak could be acoustic phonon replicas of the no-phonon peak. Note, however, that the LO replicas of the

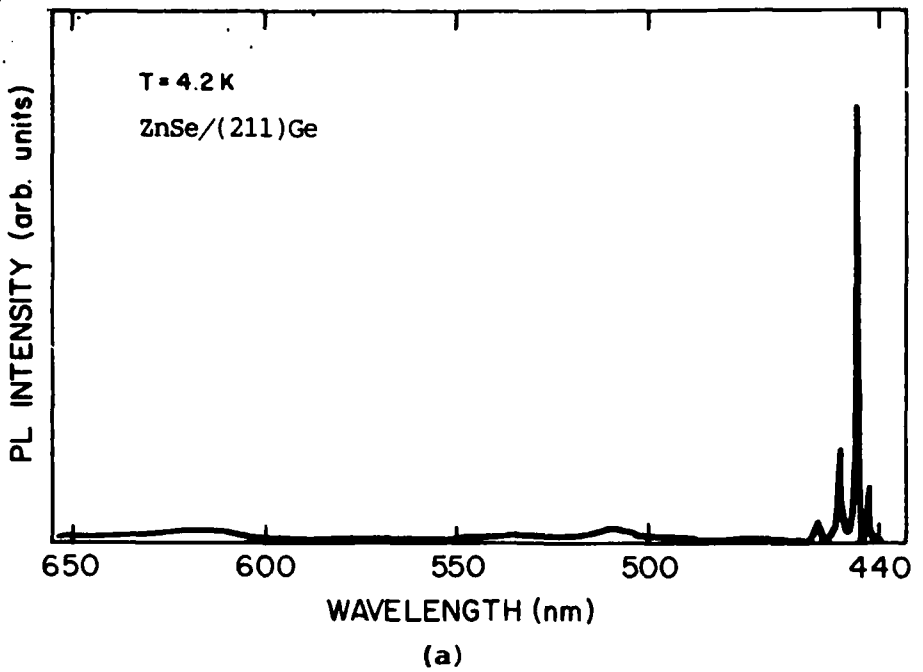

(a)

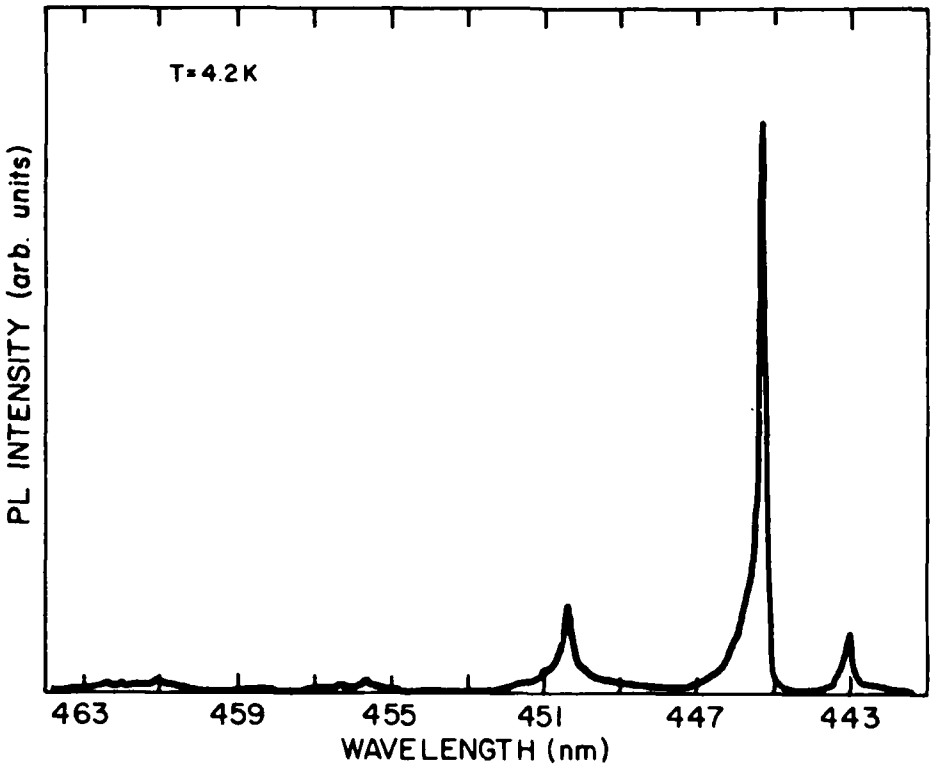

(b)

Figure 2-15. (a) Low-Temperature PL Spectrum Of ZnSe Layer Grown On (211) Ge Substrate. (b) Shows The Near Band-Edge Emission In Greater Detail.

$I_1^{d\bullet\bullet p}$ and the shoulder are resolved and are comparable in amplitude. This suggests that the shoulder is unrelated to $I_1^{d\bullet\bullet p}$ and is possibly the much weakened peak, I_1, normally observed in our layers resolved at 2.777eV. Except for the I_2 peak at about 2.798eV, the spectrum of Figure 2-15(b) is virtually clean.

2.1.4 ZnSe/GaAs Interface Structure Characterization

2.1.4.1 Cross-Section Conventional Transmission Electron Microscopy (CTEM)

A CTEM investigation of ZnSe/GaAs interfaces for a number of samples grown at different flux ratios was conducted. The main conclusion from this study is that the different flux ratios used in the study do not affect strongly the formation of defects. No clear trends were found.

For thin films, $\Delta x \leq 0.2\mu m$, the interface between the film and the substrate was smooth. However, going to thicker films, $\Delta x \geq 0.37\mu m$, a periodic strain field was found along the interface. Figure 2-16 shows two interfaces between ZnSe and GaAs for different thicknesses of the films. Figure 2-16(A) represents a film about $1.3\mu m$ thick. The strain field discussed above is clearly seen along the interface. It is thought that this strain field is associated with dislocations which are formed in thicker films upon the relief of the strain associated with the mismatch. A rough calculation of the field induced by misfit dislocations in the ZnSe/GaAs system corresponds well to the strain field as found in our samples. Figure 2-16(B) is an example of a thin film layer ($\Delta x \approx 0.2\mu m$). As can be seen, the interface is smooth without the strain field present in Figure 2-16(A). Note, also, the large number of dislocations in the interface region of the sample in Figure 2-16(A), which are absent in the thinner sample of Figure 2-16(B).

The observations in CTEM on the "critical thickness" effect and creation of misfit dislocations above the critical thickness were confirmed by studies done with double crystal and single crystal x-ray diffractometers and briefly discussed below.

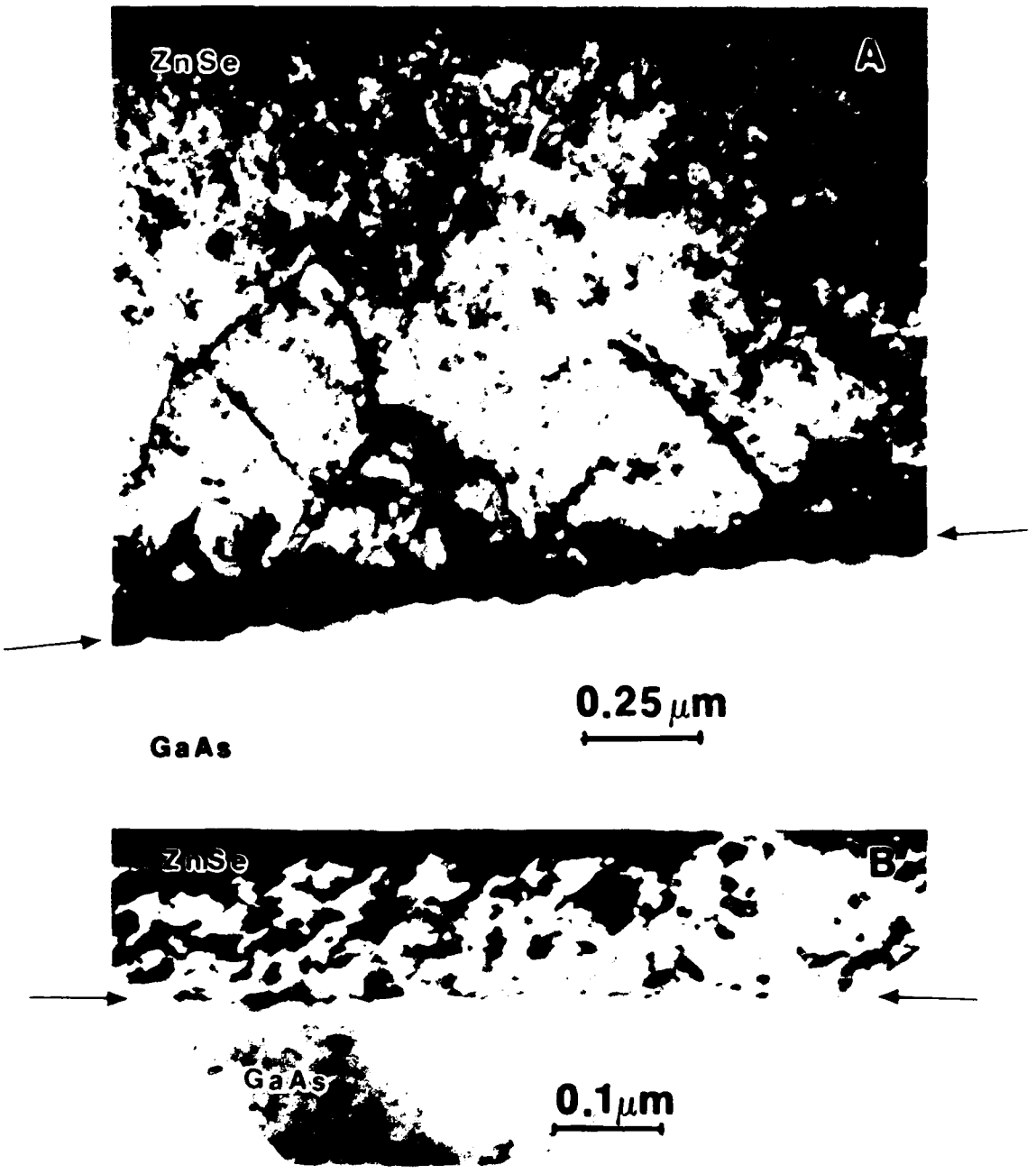

Figure 2-16. Cross-Sectional Conventional Transmission Electron Micrographs Of Two Layers Of ZnSe On GaAs. The Interface Is Shown By Arrows.

2.1.4.2 X-Ray Analysis

The analysis of a number of ZnSe/GaAs samples with single crystal and double crystal x-ray diffractometers was conducted in cooperation with Dr. Qadri of the Naval Research Laboratory in Washington, D.C. Data was obtained on the lattice constants of ZnSe and GaAs in the plane of the interface and normal to the plane of the interface using two sets of diffracting planes (400) and (224) and different angles of incidence. Good correlation between the amount of tetragonal distortion in the film and the thickness of the film was found. Figure 2-17 shows how the tetragonal distortion of the film, defined as $(a_1 - a_{11}) / \bar{a}$ where a_1 is the lattice parameter of ZnSe as measured normal to the interface, a_{11} is the lattice parameter of ZnSe measured in the plane of the interface, and a is the lattice parameter of GaAs, decreases with film thickness. As can be seen from Figure 2-17, the tetragonal distortion of the film vanishes around a thickness at 0.4-0.5μm, leaving the film in the cubic structure. This observation is in reasonably good agreement with the film thickness values found from CTEM observations, as discussed above, where misfit dislocations are introduced.

Figure 2-18 shows a set of double crystal rocking curves as measured for different film thicknesses [the thickness of the film (X) is shown (in μm) in the upper right corner of each graph]. The peak on the right is due to the ZnSe layer, the one to the left of it is GaAs related. As can be seen with thicker layers, the ZnSe peak becomes relatively stronger. Because of the relief of stress in the interface, the distance between the GaAs and ZnSe peaks also changes reflecting the fact that their lattice parameters are changing. The FWHM of ZnSe for thicker films approaches the value of 120", which was predicted as the theoretical limit for a system "substrate/film" with a mismatch of $\simeq$0.25% This observation implies that our films are of good quality with most of the broadening of ZnSe peak due to the basic "built-in" mismatch between GaAs and ZnSe.

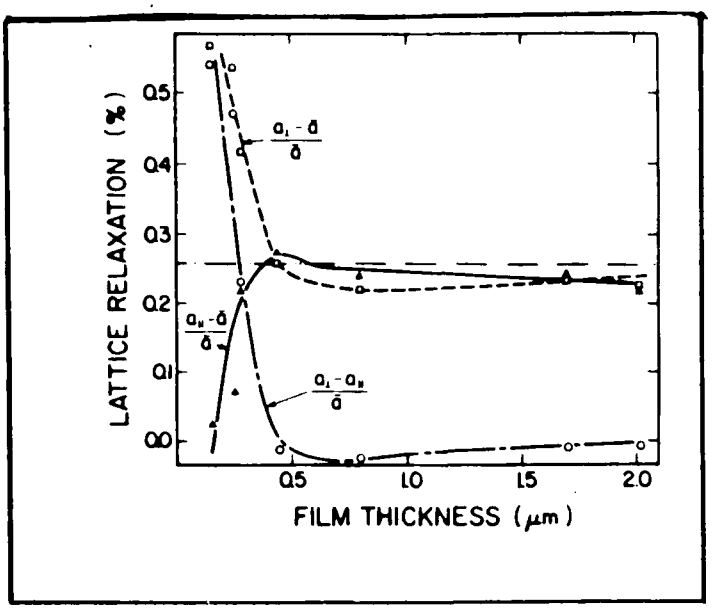

Figure 2-17. Results Of X-ray Measurements Of Lattice Relaxation In ZnSe For Different Film Thicknesses.

2.1.5 SIMS Analyses Of ZnSe/GaAs And Zn Starting Material

SIMS analyses of samples and of starting materials are being performed in order to determine the nature, concentration and sources of electrically active impurities. The analyses are performed using the Cameca IMS 4F secondary ion mass spectrometer.

To date, most of the SIMS effort has concentrated on determining the concentrations of gallium and of indium in the films, since these elements are donor species and are present during the film growth process--Ga in the substrate and In as the bonding agent between the GaAs substrate and the molybdenum block. Some efforts to determine the Al concentration have also been made, since other workers have found evidence of aluminum contamination in ZnSe grown by vapor phase transport and OMVPE [3,4]. Analyses for these elements were carried out using an O_2^+ primary ion beam of about 300nA rastered over a 250 micron square area, with a resulting milling rate of about 0.05 micron/min in ZnSe. Positively charged secondary ions were detected at mass 27 for Al, 69 and 71 for Ga, and 113 and 115 for In.

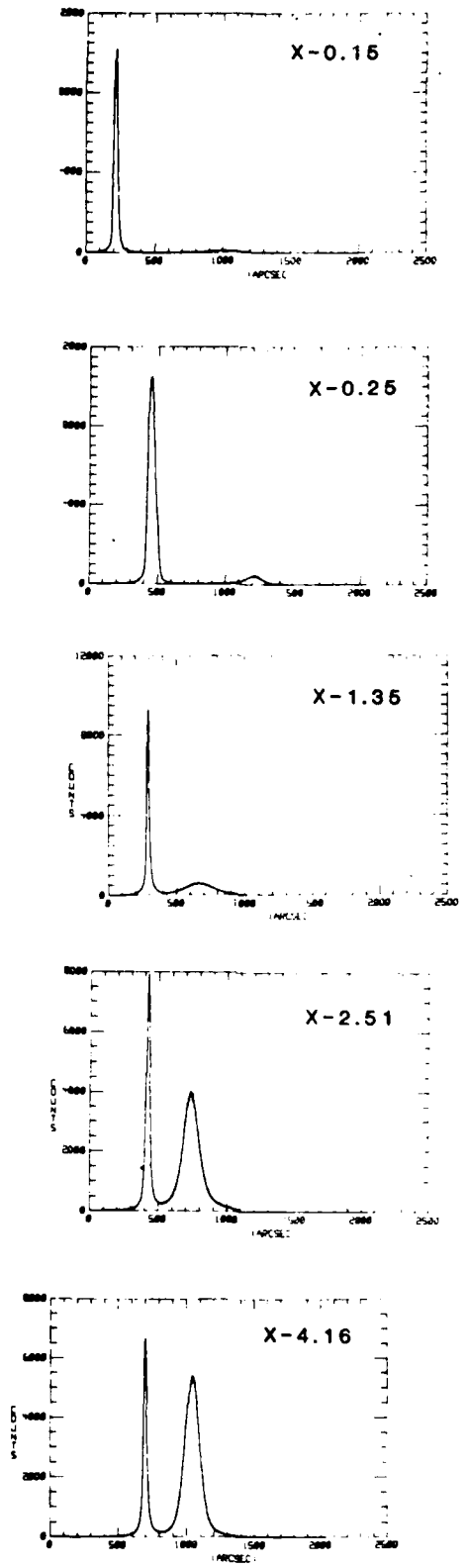

Figure 2-18. Results Of Double Crystal Rocking Curve Measurements For A Set Of Samples With Different Film Thicknesses (Shown In μm In The Upper Right Corner Of Each Graph).

The ratio of the mass 69 signal to the 71 signal was found to be larger than that expected from the natural abundances of the Ga isotopes. This was attributed to mass interference from the ZnH molecular species. It has not been possible to resolve the separate interfering contributions to the mass 69 or 71 signals, by either voltage offset or high mass resolution techniques. Therefore the mass 71 signal was used to provide an upper bound on the Ga concentration.

For the case of the In isotopes, the ratio of the mass 113 signal to the 115 signal was found to be enhanced with respect to the expected value. In this case, the enhancement is probably due to the fact that the 115 signal (the more abundant isotope) is already nearing the background count rate, so that the 113 signal suffers a proportionally larger enhancement due to background. For this reason, the mass 115 signal was used to provide an upper bound for the In concentration.

To date, mass interferences which are suspected in the mass 27 signal have not been characterized.

For quantification of the SIMS results, standards were produced by ion implantation of the relevant species into MBE-grown ZnSe films. The implanted species were Al^{27}, Ga^{71}, and In^{115}. Implantations were performed at 200KeV, with peak concentrations of the implanted species reaching $1.0x10^{18}cm^{-3}$. Secondary ion yields were calculated by integrating the entire SIMS profile of the standard sample and using the known implantation dose. Calibration factors derived from the implantations were in fair agreement with those derived from the pressed powder samples. For a given signal strength, the implantation calibrations yield about 0.22 X the Ga concentration of the powder calibration, and about 0.10 X the In concentration of the powder calibration. The implantation calibrations are felt to be more reliable due to the stable signals obtained from the implanted samples, and due to the more realistic local chemical environment experienced by the implanted species.

The maximum Ga, In and Al concentrations determined by the above method for samples ZSE12, 13, 14, and 15 are found in Table 2-3. These values correspond to analyses of approximately the first micron of the films. Also shown are the growth temperature, Zn:Se beam pressure ratios, film

thicknesses and the total donor concentrations as determined by temperature-dependent Hall measurements. This series of samples was chosen for analysis because the samples were grown under conditions which were identical except for the Zn:Se beam pressure ratio. (Additional data on these films can be found in Six Month Technical Progress Report No. 1).

TABLE 2-3. SIMS Upper Limits On Ga, In and Al Concentrations

SAMPLE	Tg (°C)	BEP_{Zn}/BEP_{Se}	t (μm)	N_D (cm^{-3})	[Ga] MAX (cm^{-3})	[In] MAX (cm^{-3})	[Al] MAX (cm^{-3})
ZSE12	350	0.30	1.4	$2.2x6^{17}$	$1x10^{15}$	$7x10^{13}$	$1x10^{15}$
ZSE13	350	0.36	1.6	$9.0x10^{16}$	$2x10^{15}$	$7x10^{14}$	$8x10^{15}$
ZSE14	350	0.88	2.4	$7.1x10^{16}$	$8x10^{15}$	$3x10^{14}$	$3x10^{16}$
ZSE15	350	1.92	2.3	$2.5x10^{16}$	$1x10^{15}$	$3x10^{14}$	$5x10^{15}$

The important point to notice is that, in all cases, the maximum concentrations of Ga and In estimated on the basis of the implanted standards are at least an order of magnitude smaller than the measured donor concentrations. If the powder calibrations are used, then the above statement is still true for samples ZSE12 and 13, but the combined Ga and In concentrations approach the measured donor concentration in samples ZSE14 and 15 to within a factor of 2-3. It may therefore be stated with confidence that Ga and In are not the dominant donor species in ZSE12 and 13. It is, however, possible, though unlikely, that they contribute significantly to the donor concentration in ZSE14 and 15.

The maximum Al concentration, although insignificant in films ZSE12 and 13, is comparable to the total donor concentration in samples ZSE14 and 15. This may imply that some type of source material purification will be needed to reduce the aluminum contamination of the films. However, several points should be emphasized. First, the results on Al are based on a relatively small number of analyses, in contrast to the results for In and Ga. Second, mass interferences have not been well characterized for Al; it is likely that there is at least some contribution from a CN interference. Such an

interference could account for the relatively large and apparently non-systematic variation of the observed Al signal.

In addition to the quantitative efforts above, survey mass spectra were taken on the films using both the Cs^+ and O_2^+ primary beams. Elements other than Al, Ga and In which have been positively identified in the films include Cu, F, and Cl. However, these impurities have not yet been quantified. Species which should be easily detectable and appear to be absent include Li, Na, K, Ti, Cr, Mn, B, Si, Ga, As and Br.

Starting material SIMS analyses have, to date, concentrated on metallic impurities in the Zn. The Zn shot source material was pressed in a hydraulic press to form platelets suitable for analysis. SIMS spectra indicated that any Ga contamination is at present totally obscured by the ZnH interference. There is no detectable In. A potentially significant Al signal is observed, but the Al concentration has not yet been quantified.

In the next quarter, efforts to better quantify the SIMS analyses and to correlate the results with other properties of the films will continue. Mass interferences in the Al signal will be studied, and implanted standards for Cu, F and Cl will be obtained.

2.1.6 Theoretical Study of Electron Mobility in a 2DEG Confined at a Lattice-Matched ZnSe-Zn(S,Te) Heterointerface

Although the semiconductor ZnSe has a direct bandgap in the blue visible spectral region, progress toward integrated electro-optical devices in the visible using this material is hampered by its relatively poor transport properties. One means of achieving higher electron mobilities in such materials is to employ a two-dimensional electron gas (2DEG). A limitation on the formation of a 2DEG at a heterostructure interface is that the two materials be closely lattice-matched. The relief of interfacial strain at mismatched heterostructure interfaces results in the formation of misfit dislocations and other defects; a fraction of these defects will be charged. In the case of a two-dimension electron gas confined at a single quantum well (SQW) heterointerface, these fixed charges can efficiently scatter electrons, limiting their mobility. A perfect lattice-matched heterointerface in principle eliminates this problem allowing for inherently

faster electron transport. With regard to forming a 2DEG in ZnSe, a promising candidate material for lattice-matching is ZnSTe. Here, a lattice-matched ZnSe-$ZnS_{1-x}Te_x$, x=0.37 heterointerface is proposed as a means of confining a 2DEG in ZnSe.

The transport properties of electrons in the 2DEG were calculated for the first time, and the dependence of the electron mobility on the well areal density at 4.2K and 77K is discussed. The proposed ZnSe-ZnSTe heterojunction is comprised of a doped region of alloy (doped to about 10^{16}-$10^{17}cm^{-3}$) separated from the interface by a layer of nominally "undoped" alloy ("spacer region") of width d.

Figure 2-19 shows the calculated electron mobility versus areal density, N_s, at 4.2K, giving the relative contributions of each of the scattering mechanisms. The inherent limit curves shown in Figure 2-20 are obtained when remote ionized impurity scattering is included. For a detailed discussion of the theoretical results, see reference [5].

2.2 Project II: Device Research

2.2.1 E-Beam Pumping

Measurements during the past quarter were hampered by repeated mechanical failures in the e-gun system which resulted in a "down time" of over two months. Nonetheless, it has been possible to extend our earlier measurements of e-beam pumped lasing in MBE-grown ZnSe films to the exploration of additional parameters (sample temperature and accelerating voltage) and to additional samples.

Using cavities cleaved from the sample reported on in our six month technical progress report [ZSE14A; t=2μm; grown on (100) GaAs thinned to 50μm and cleaved to rods 100-300μm wide], we have measured the variation in the threshold current density and the lasing wavelength with cold finger temperature. [See Figure 2-21(a).] A rather slow variation for T < 100K is not unexpected as the sample temperature in the pumped region rises very rapidly when the starting temperature is less than 50K; i.e., the real

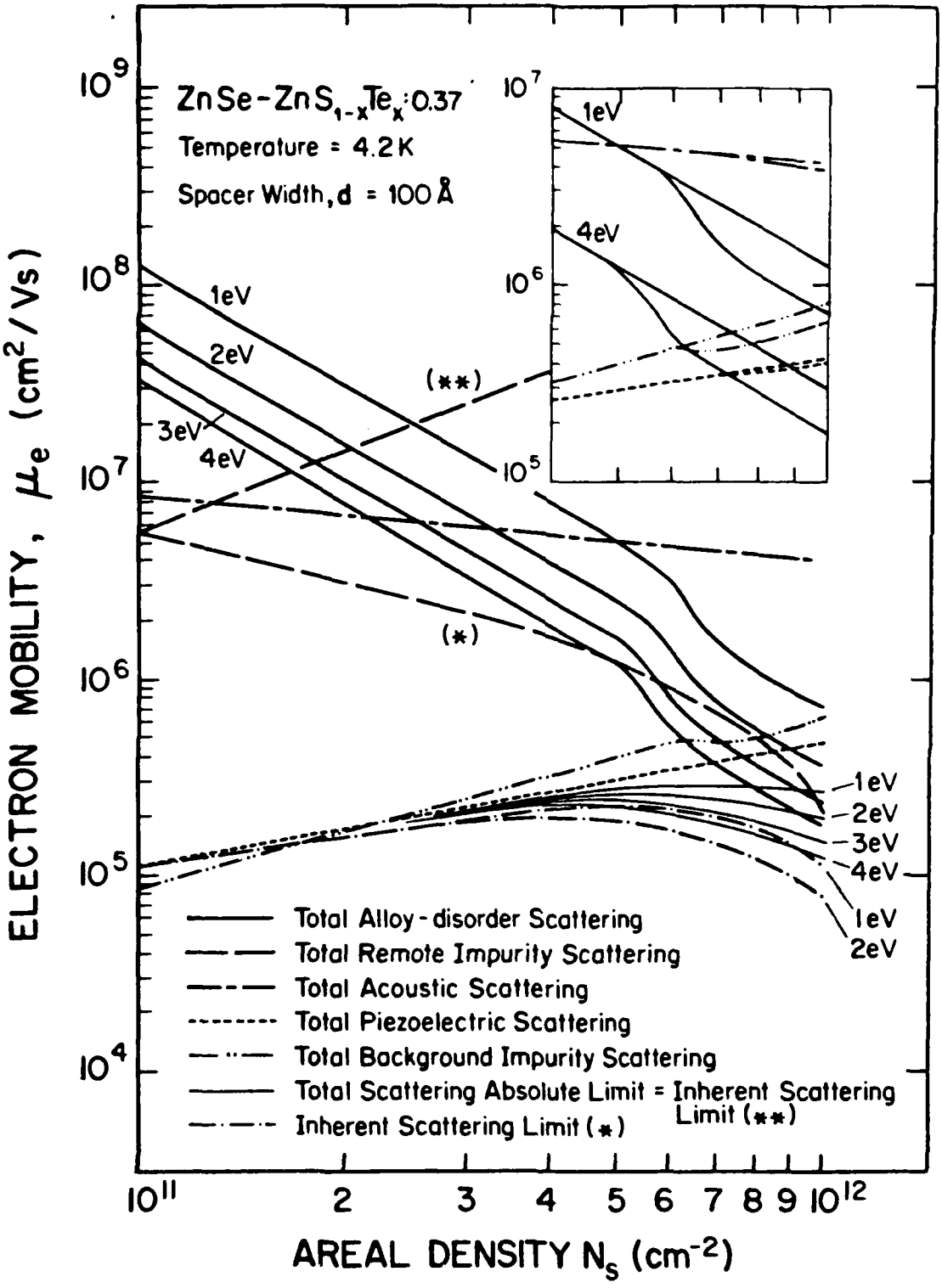

Figure 2-19. Electron Mobility In A 2DEG As A Function Of Areal Density, N_s. Contributions From Various Scattering Mechanisms Are Shown.

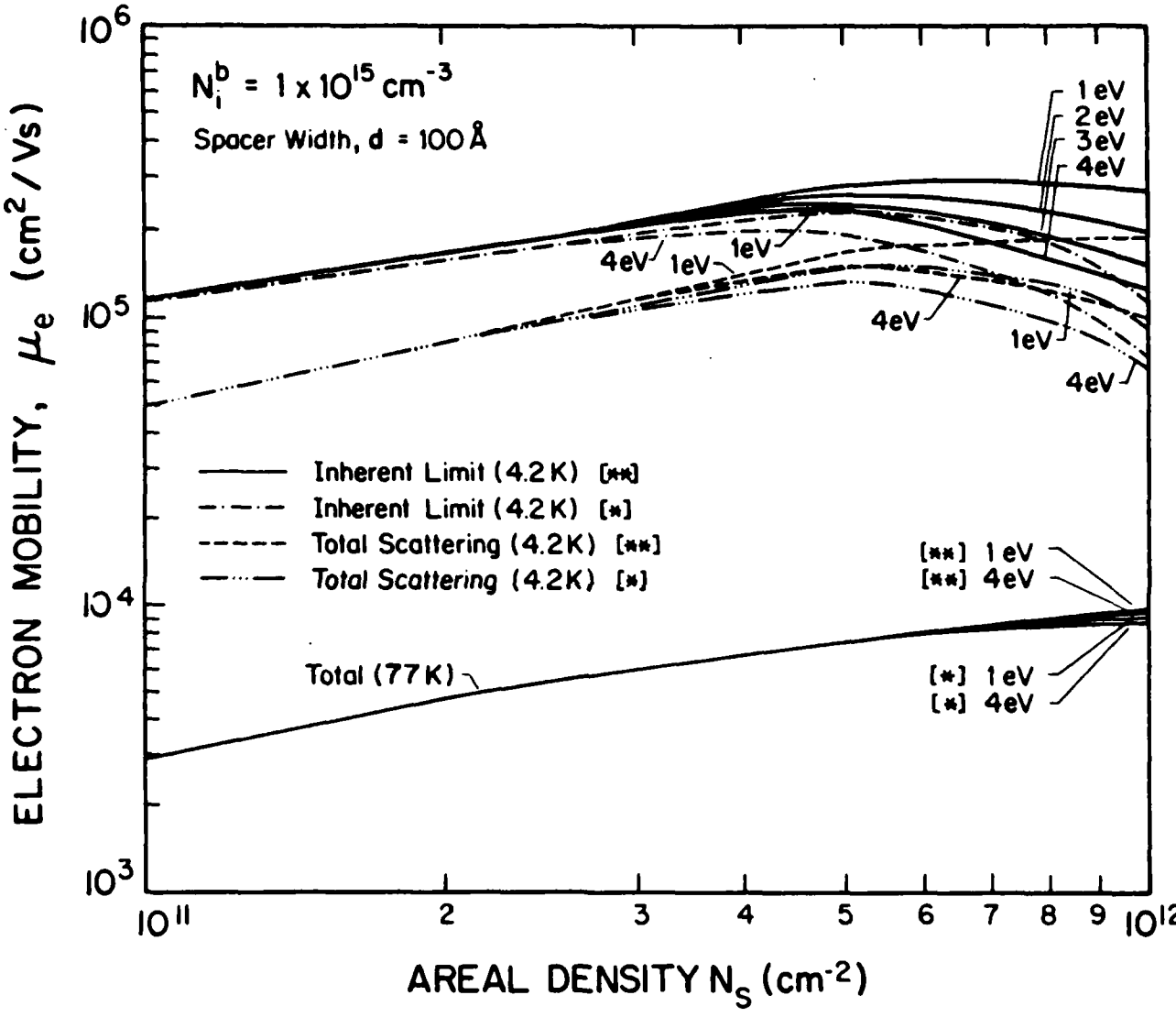

Figure 2-20. Inherent Limit Of Electron Mobility In A 2DEG At 4.2K Is Shown As A Function Of Areal Density N_s.

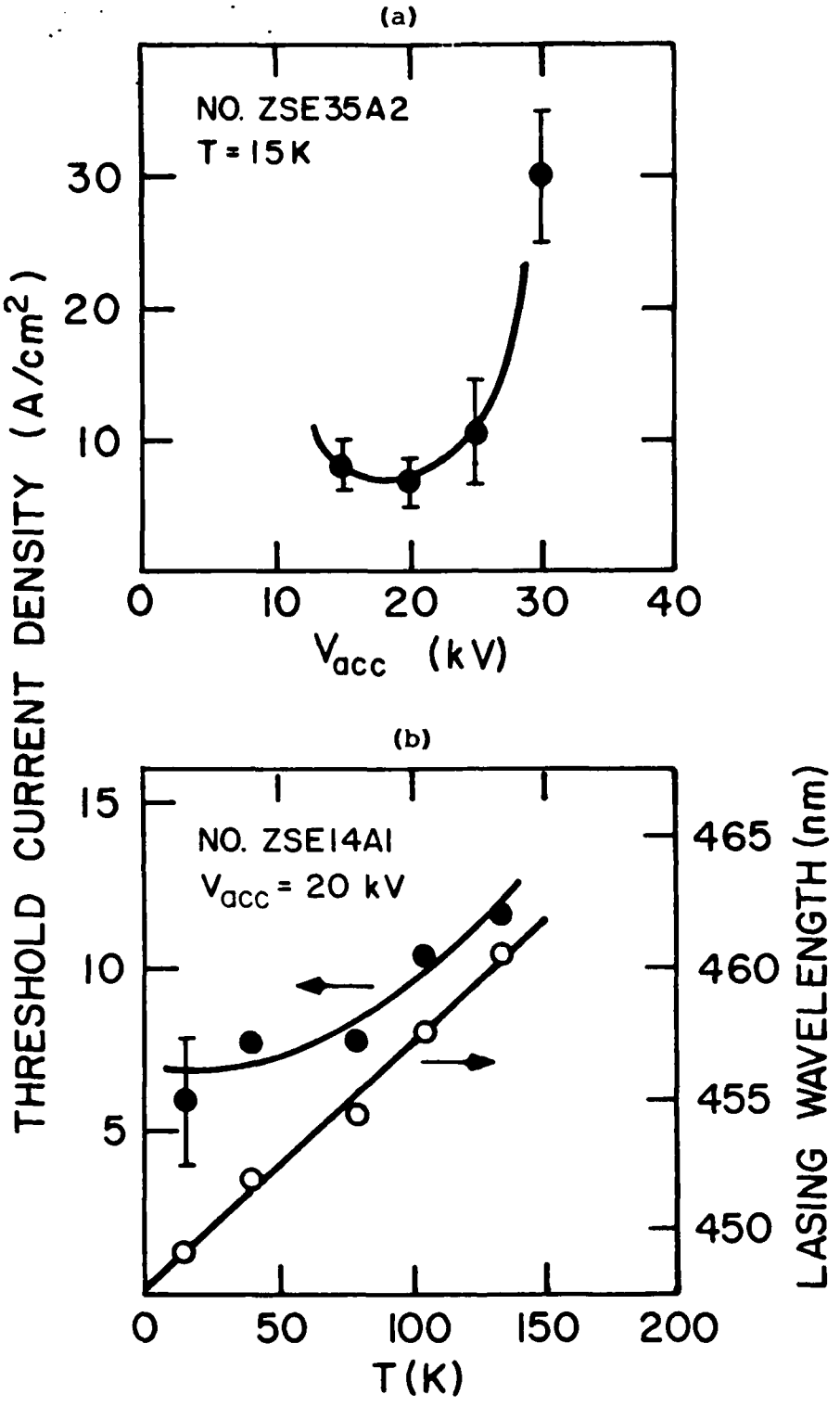

Figure 2-21. (a) Variation Of Threshold Current Density And Lasing Wavelength With Cold Finger Temperature. (b) Variation Of Threshold Current Density With e-Beam Energy.

temperature in the gain region is similar for all "cold finger" temperatures < 100K. The curve shows a rapid rise for T > 150K, reflecting our inability to pump the samples to lasing at these temperatures, even when using $J=20A/cm^2$. The variation of the lasing wavelength with T is more rapid than expected on the basis of bandgap variation; it may indicate a change in the lasing mechanism as the temperature is increased.

In Figure 2-21(b) we show the variation of J_{th} with accelerating voltage. In bulk material, the threshold is expected to decrease monotonically with increasing accelerating voltage. Because our films are only 2μm thick, as the accelerating voltage increases, more of the energy is deposited in the GaAs substrate, thereby raising the threshold. Qualitatively, then, we expect to observe a minimum in the J_{th} vs. V_{acc} curve. All of the results shown in Figure 2-21 are preliminary; much more detailed and careful experiments will be done to quantify these ideas.

We have prepared cavities from one of our recently-grown MBE ZnSe samples [ZSE37A; 2μm thick on (100)GaAs thinned to 20-100μm; cavity widths 150-450μm]. Several of these cavities were attached to the cold finger of the closed-cycle refrigerator using a Ga-In eutectic. This was done in order to eliminate any thermal shock to the cavity during the In soldering step. We have pumped several of these cavities to lasing at threshold currents comparable to, but slightly higher than, those found for ZSE14A. No systematic dependence of lasing threshold on cavity length has yet been seen.

We have performed a preliminary, and very crude, estimate of the efficiency of our e-beam pumped ZnSe laser by collecting as much of the output beam as possible with an integrating sphere. Taking the measured output and correcting for collection geometry, window reflection, and detector efficiency, we estimate an external efficiency (i.e., e-beam power in/light power out) of 1.5%.

We have been concerned about the large spectral widths (>6A) of our lasing peaks. This is due in part to a lack of resolution in our spectrometer/OMA system. We suspect that there is also some broadening and shifting resulting from heating and/or band-gap renormalization during the e-beam pulse. This is demonstrated in Figure 2-22(a) through (e) where a

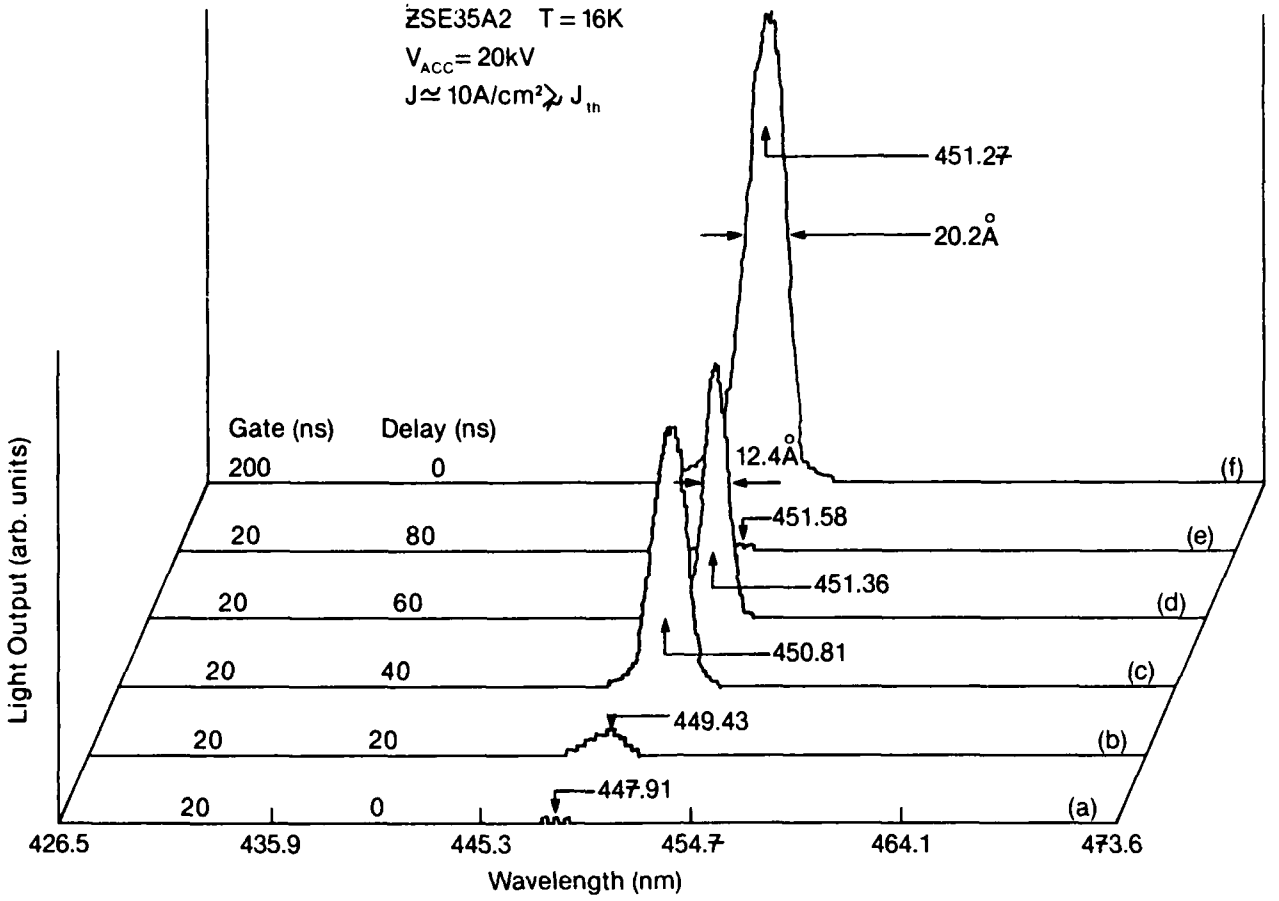

Figure 2-22. Effect Of Moving A 20ns OMA Gate Through The Duration Of the Pulse.

short (20ns) OMA gate is moved through the duration of the pulse. Compare these to those of Figure 2-22(f) which used a 200ns OMA gate covering the entire 100ns light output--this gives a convolution of the Figure 2-22(a) through (e) spectra. The lasing wavelength variation with time obtained from these measurements is shown in Figure 2-23. There we also show our calculation of the wavelength shift resulting from heating of the ZnSe by the e-beam pulse; there is a rapid initial rise from T=15K due to the small low-temperature heat capacity, but the temperature rise (and, therefore, the wavelength shift) quickly levels off with time. It is clear that our observed shift cannot be accounted for by heating alone. There is a sizeable contribution from band-gap renormalization. We are continuing to investigate this experimentally and theoretically.

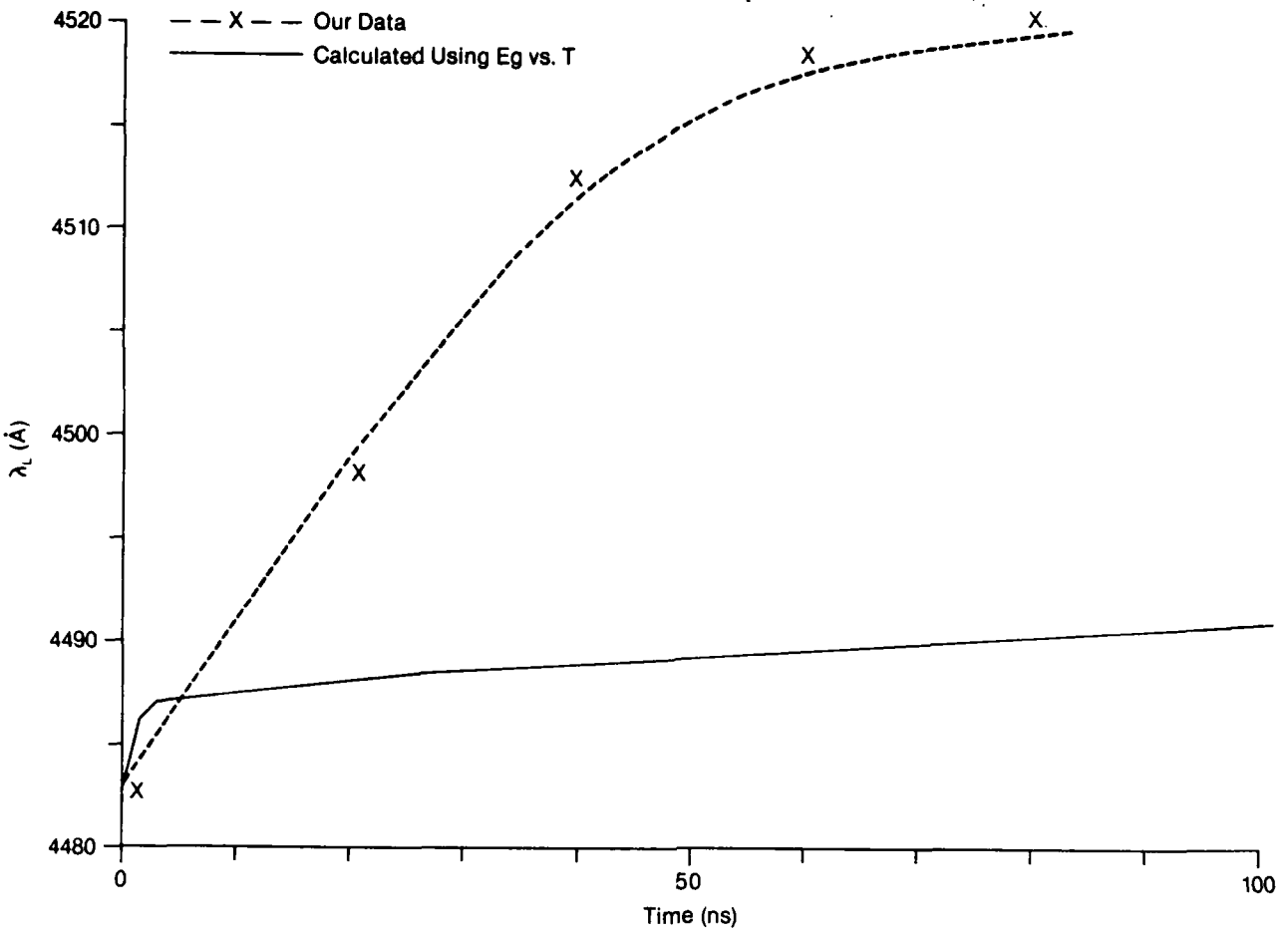

Figure 2-23. Lasing Wavelength Variation With Time.

2.3 Project II, Task 2: Contact Studies

2.3.1 Contacts - Ohmic And Schottky

The purpose of the present contact studies is twofold: (i) to understand and characterize the formation of ohmic and Schottky contacts on ZnSe, and (ii) to improve the adhesion of contacts to ZnSe for subsequent wire bonding during device fabrication.

2.3.1.1 Ohmic Contacts

In order to understand ohmic contact formation, planar In electrodes were evaporated on ZnSe grown on SI-GaAs. Current-voltage measurements were made between the electrodes. As deposited, In gave rectifying contacts. With subsequent annealing for 24 minutes at 300°C (in Ar/5% H_2), there was some improvement. Resistivity, measured at 300K in this two-electrode configuration, was four times higher than that obtained by Hall measurements. This might be attributable to a non-ohmicity of the contacts. With prolonged annealing, the ohmicity of the contacts degraded. We have initiated Auger depth profiling studies on these samples. Our preliminary results indicate a significant indium diffusion in the ZnSe. Systematic studies of In diffusion will be reported later.

2.3.1.2 Schottky Contacts

Schottky contacts are necessary for C-V and DLTS characterization of ZnSe. For Schottky barrier formation, we have studied the I-V characteristics of evaporated Au/Pd, Au/Cr, Au and Au/Al electrodes on ZnSe. Reproducibility of the Schottky contacts, in order of decreasing reproducibility, is as follows: Al, Cr, Pd, Au. Apparently more reactive metals form more reproducible Schottky barriers. All contacts were evaporated onto the ZnSe through a shadow mask. A typical Au/Al/ZnSe/N^+GaAs I-V characteristic is shown in Figure 2-24.

Ideality factors, η, ranged from 1.1 - 1.5 in most cases, over a range of current of four orders of magnitude. So far, we have not determined the barrier height from temperature dependent I-V measurements. However, C-V measurements on these diodes indicate a barrier height of 1.4 eV (Figure 2-25). This value of barrier height is substantially larger than that reported in the literature [6], and might be due to an interfacial oxide [7]. At high bias voltages, the slope of the I-V curve is observed to decrease. In the ideal diode, this behavior is due to a voltage drop (IR_s) across a series resistance in the diode. However, R_s estimated from the I-V curve is at least three orders of magnitude larger than the R_s obtained from Hall measurements. We believe that this discrepancy results from the presence of an interfacial oxide layer at the metal/ZnSe interface. The

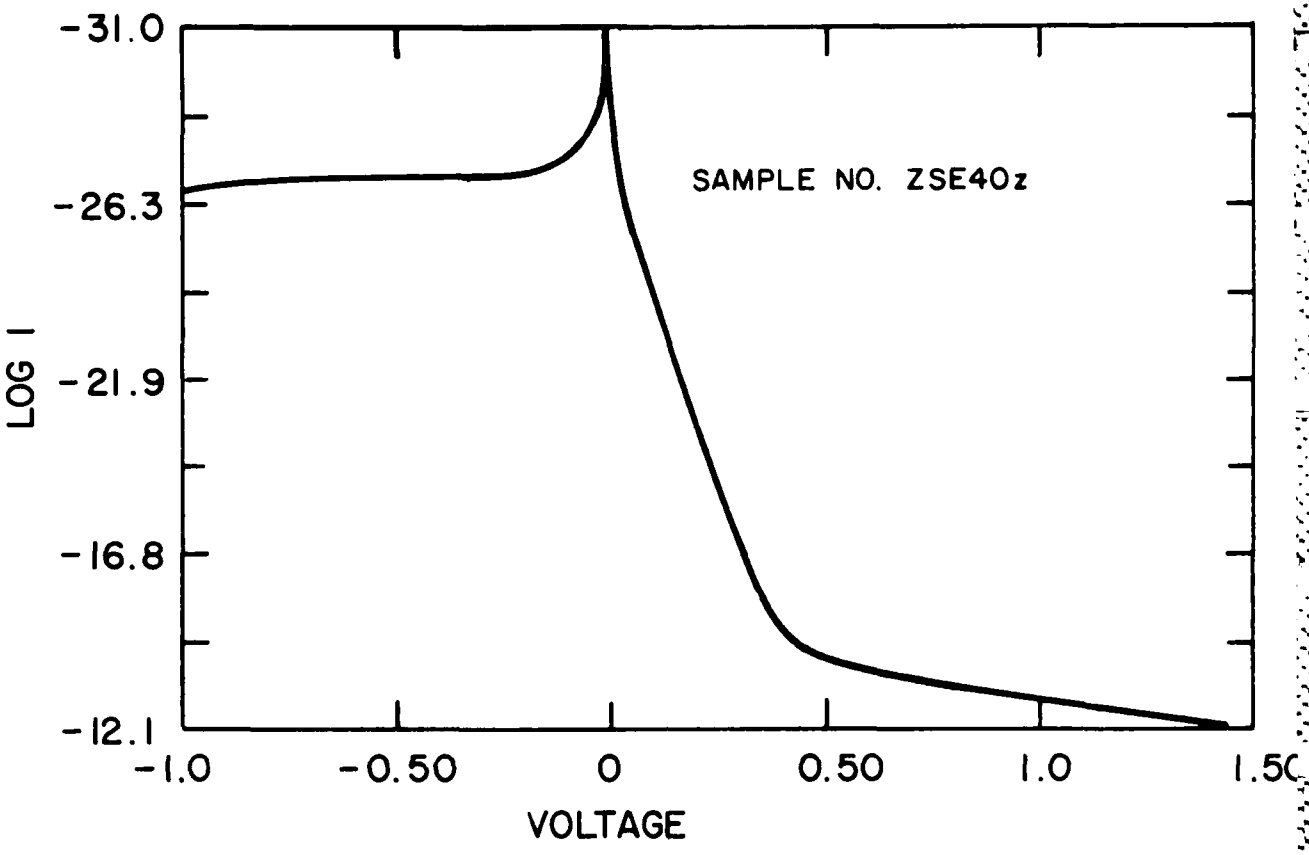

Figure 2-24. Current-Voltage Characteristics Of N^+ GaAs/ZnSe/Al Schottky Barrier Diode AT 300K.

interfacial oxide layer can be eliminated by depositing the Schottky contact inside the MBE system. Such an in situ metallization facility is currently being built.

2.3.2 C-V Measurements

In order to measure the carrier concentration, distribution and Schottky barrier height, C-V measurements have been initiated. At present, we are concentrating on aluminum Schottky barriers on ZnSe because of the better reproducibility in contact characteristics. In some of the Schottky diodes, we have varied the depletion width by as much as 2μm with a reverse bias voltage of 40V. So far, we have used C-V measurements to evaluate the

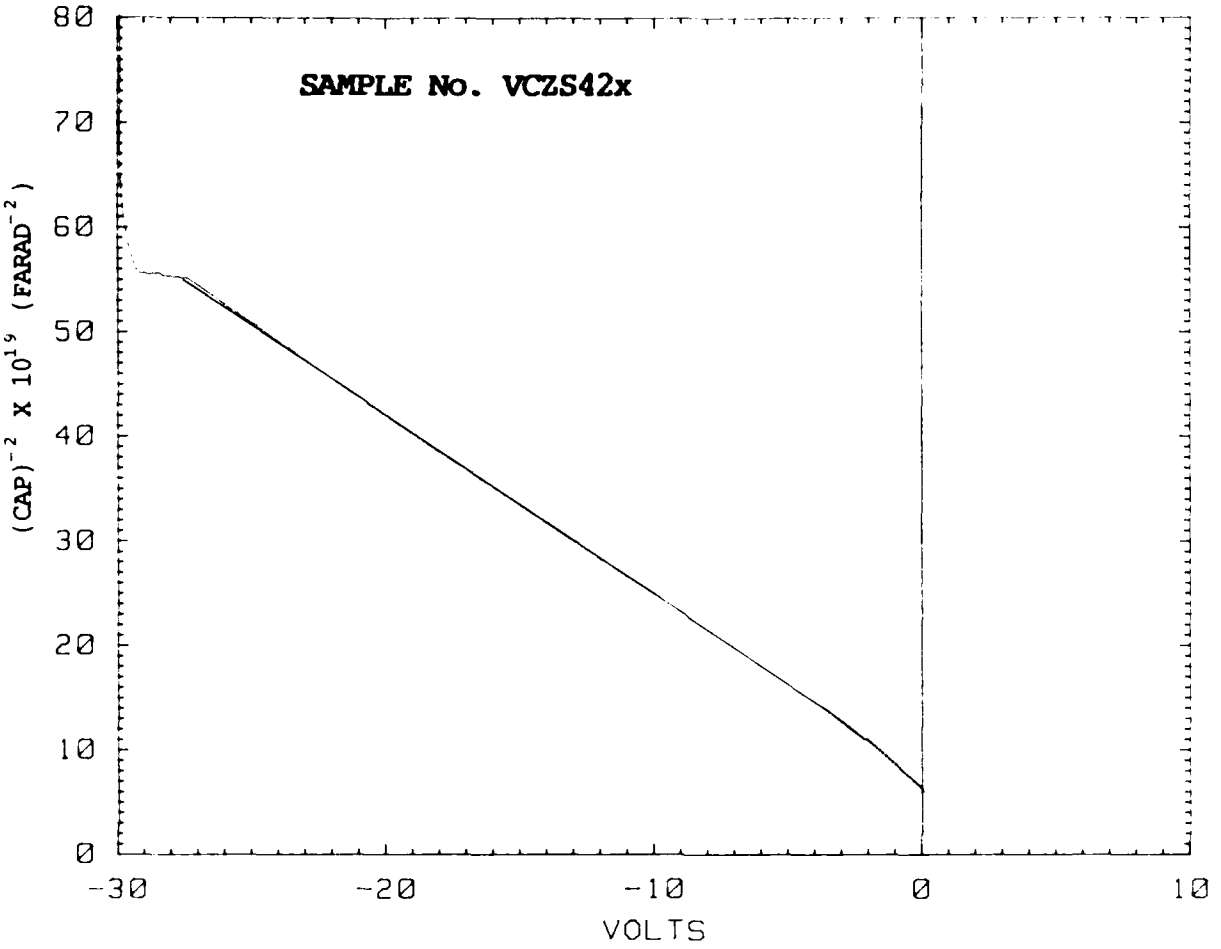

Figure 2-25. $1/C^2$ Versus Voltage For A Typical N^+ GaAs/ZnSe/Al Diode.

local electron concentration in ZnSe and the Schottky barrier height of the meta_ contact. The local electron concentration $N_D^+ - N_A^-$ can be estimated in the depletion layer approximation from the slope of $1/C^2$ vs. V measurements. $N_D^+ - N_A^-$ is given by,

$$N_D^+ - N_A^- = \frac{2}{qEA^2} \qquad \frac{dV}{d\,(1/C^2)}$$

where $N_D^+ - N_A^-$ are densities of ionized donors and acceptors respectively, C is the capacitance of the depletion layer, V the voltage, A the contact area of the Schottky barrier and ε is the dielectric constant (9.12) of

ZnSe. A linear $1/C^2$ vs. voltage indicates a uniform doping profile. Typical $1/C^2$ vs. V plots and the corresponding $N_D^+ - N_A^-$ versus depth, x, are shown in Figures 2-25 and 2-26, respectively. The carrier concentrations at 300K calculated from Hall and C-V measurements are shown in Table 2-4. We observed a good correlation between the Hall and C-V measurements. From C-V profiling studies we have obtained the distribution of carriers throughout the ZnSe film. In some samples, the concentration has been observed to change from the bulk to the surface by an order of magnitude. Such an impurity distribution is not well understood at this moment. Wherever such a distribution exists, an average value of $N_D^+ - N_A^-$ was taken.

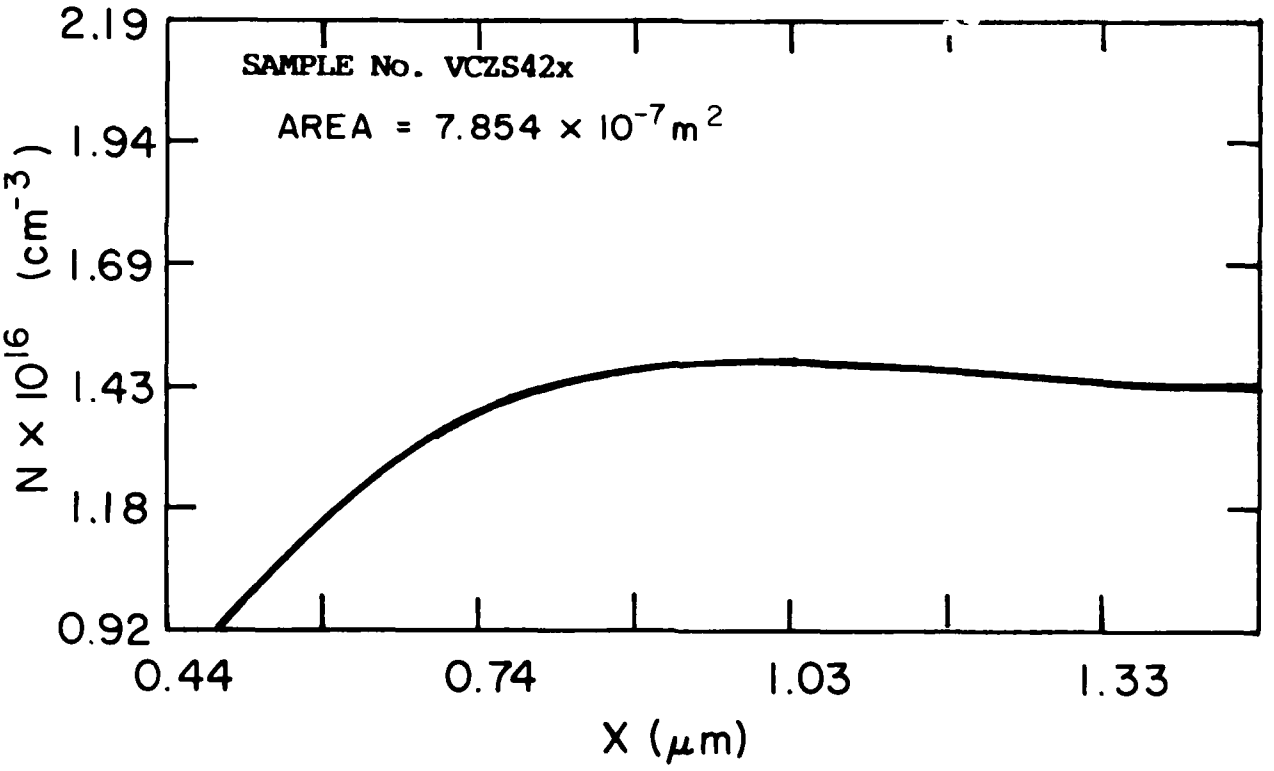

Figure 2-26. Depth Distribution Of Electron Concentration In N^+ GaAs/ZnSe/Al Diode.

TABLE 2-4. Comparison Of Carrier Concentrations Calculated From Hall And C-V Measurements

SAMPLE	CONTACT METAL ZnSe/M_1/M_2/M_3	300K (CM^{-3}) HALL ($N_D^+ - N_A^-$)	CAPACITANCE
4B(1)	Al/Au	1.9×10^{17}	1.26×10^{17}
4B(2)	Al/Au	1.9×10^{17}	5.3×10^{16}
11B	Al/Au	5.36×10^{16}	5.3×10^{16}
14B	Al/Au	2.0×10^{16}	2.3×10^{16}
26B	Cr/Pd/Au	1.1×10^{16}	9.0×10^{15}
26B	In/Au	1.1×10^{16}	1.2×10^{16}
27B	Au	1.5×10^{16}	1.0×10^{16}
29B	Cr	1.5×10^{16}	1.8×10^{16}
29B	Pd	1.5×10^{16}	1.1×10^{16}
29B	Cr/Au	1.5×10^{16}	1.8×10^{16}
37B	Al/Au	9.6×10^{15}	9.2×10^{15}
39B	Al/Au	---	1.3×10^{15}
40B	Al/Au	3.9×10^{16}	2.4×10^{16}
41B	Al/Au	1.32×10^{16}	1.4×10^{16} (a)
42B	Al/Au	1.45×10^{16}	1.4×10^{16}
43B	Al/Au	4.82×10^{16}	4.3×10^{16}

(a) $N_D^+ - N_A^-$ increased by an order of magnitude from surface to 1.3μm deep into the ZnSe film.

Hall measurements could not be made in some of our ZnSe films because of their high resistivity. These films were grown at a T_s of 400°C. Capacitance measurements indicated complete depletion of the ZnSe at a reverse bias of only about -1V (Figure 2-27). The carrier concentration determined from $1/C^2$ vs. V was 1.3×10^{15} (ZSE 39B, Table 2-4) in one of these films. In addition to the small punch-through voltage, C-V characteristics indicated a distinct peak in the forward bias. This is not as distinct in the more conductive films. Such a behavior might be associated with a double Schottky behavior; e.g., GaAs/ZnSe and ZnSe/Al Schottky barrier interfaces. Using the photomission data of Katnari et al [8], a conduction band discontinuity ΔE_c, of 0.2 eV can be expected. The

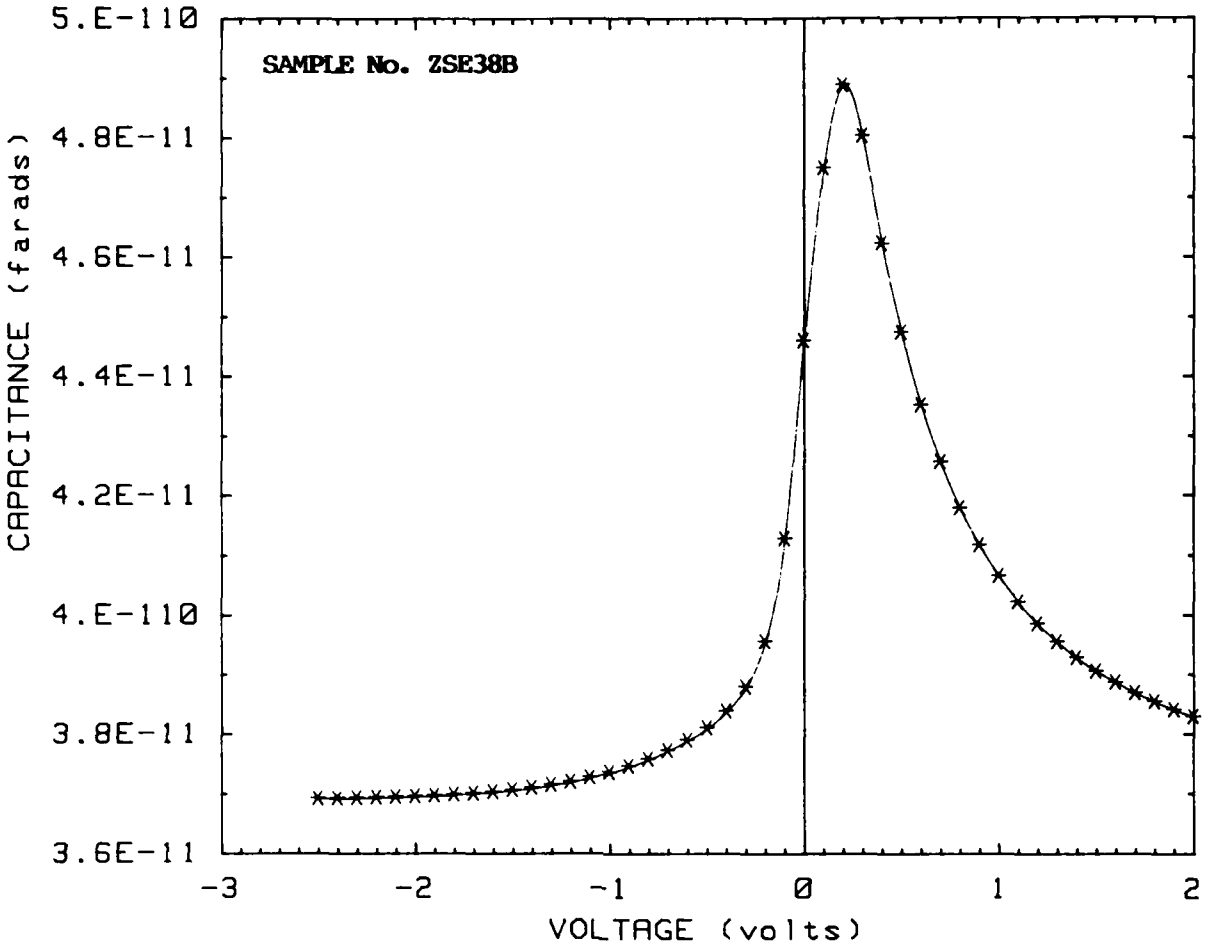

Figure 2-27. Capacitance-Voltage Characteristics Of A High Resistivity ZnSe Film.

zinc selenide side will be depleted for low resistivity films and accumulated for very high resistivity ($n<10^{14}cm^{-3}$) films. Occurrence of an interfacial barrier (GaAs/ZnSe) will be more pronounced in high resistivity films such as ZSE39B. Depletion widths in more conductive films will be smaller and tunneling assisted injection will make the semi-conductor heterojunction more injecting. This explanation is only qualitative at this point.

We are currently investigating the problem of heterojunction band discontinuity in the GaAs/ZnSe system.

2.3.3 DLTS Measurements

Three ZnSe samples ($In/N^+GaAs/ZnSe/M$) have been investigated for DLTS measurements. In two of these samples, minority carrier transients were observed, and the third sample gave a majority carrier transient with significant noise. Minority carrier transients in a Schottky diode are less likely. It is felt that some of these problems are probably associated with high leakage currents in these samples at low reverse voltage bias, and with stray capacitance. In order to isolate sample problems from system performance, we have made DLTS measurements on a calibrated Si diode (neutron irradiated) obtained from J. Farmer of the University of Missouri. Good DLTS spectra were observed as shown in Figure 2-28. The inset in the figure shows the activation energy of the traps, in good agreement with previously measured values supplied to us. Therefore, our current problems associated with DLTS measurements on ZnSe are associated with the ZnSe sample itself; we are presently investigating possible solutions.

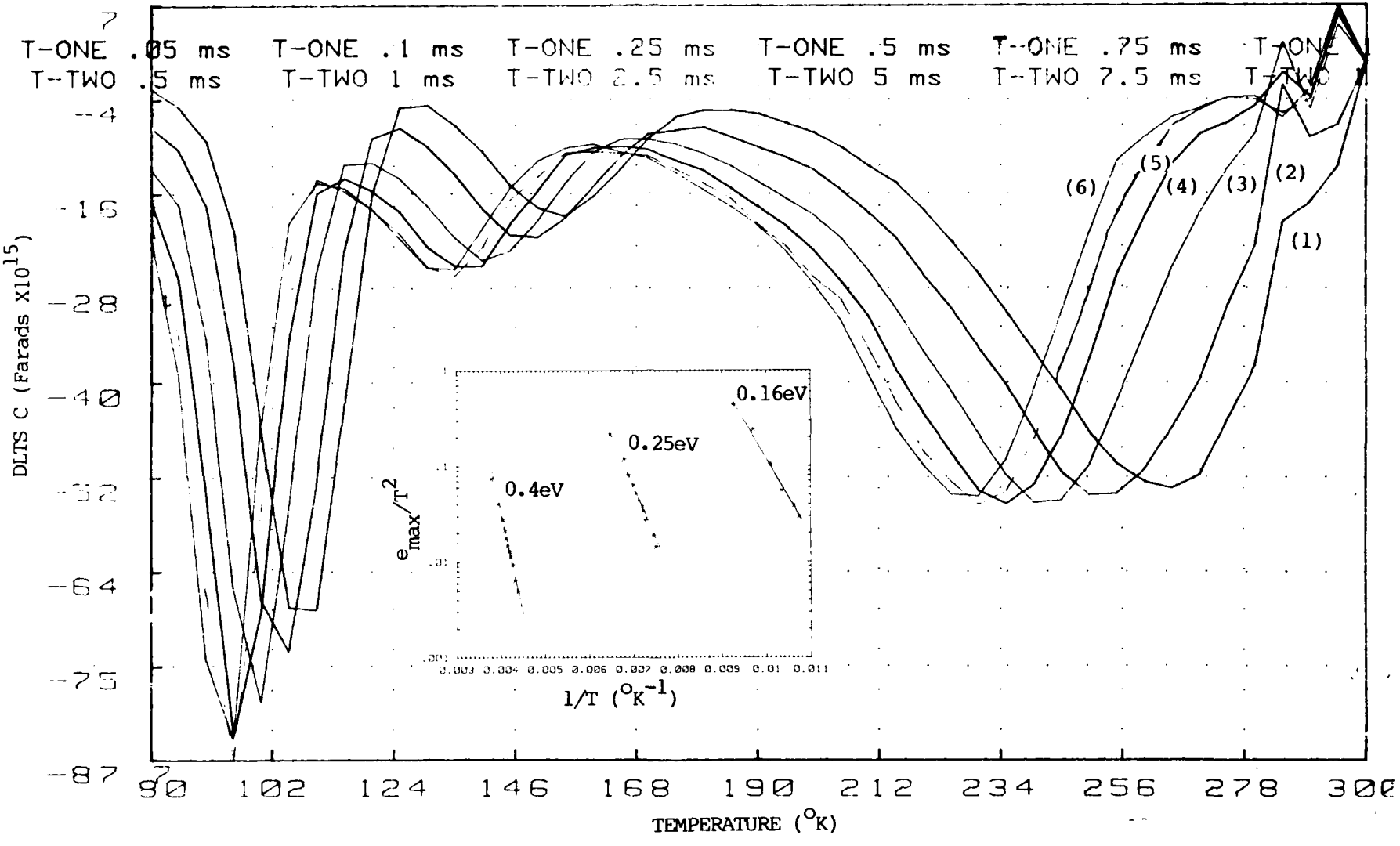

Figure 2-28. DLTS Spectrum Of A Si-Diode. Inset Shows The Activation Energy Plots Of Three Traps In The Si Diode.

3.0 REFERENCES

1. R. M. Park and H. A. Mar, to be published in Journal of Materials Research.

2. R. M. Park and H. A. Mar, Appl. Phys, Lett., 48(8),529(1986).

3. J. L. Merz, H. Kukimoto, K. Nassau, and J. W. Shiever, Phys. Rev. B, 6,545(1972).

4. S. Fujita, T. Yodo, and A. Saski, J. Cryst. Growth, 72,27(1985).

5. H.E. Ruda, to be published in Applied Physics Letters.

6. R. K. Swank, M. Aven, and J. Z. Devine, J. Appl. Phys., 40,89(1969).

7. S. J. Fonash, J. Appl. Phys.,54,1966(1983).

8. A. D. Katnani and G. Margaritondo, Phys. Rev. B,24, 1944(1956).

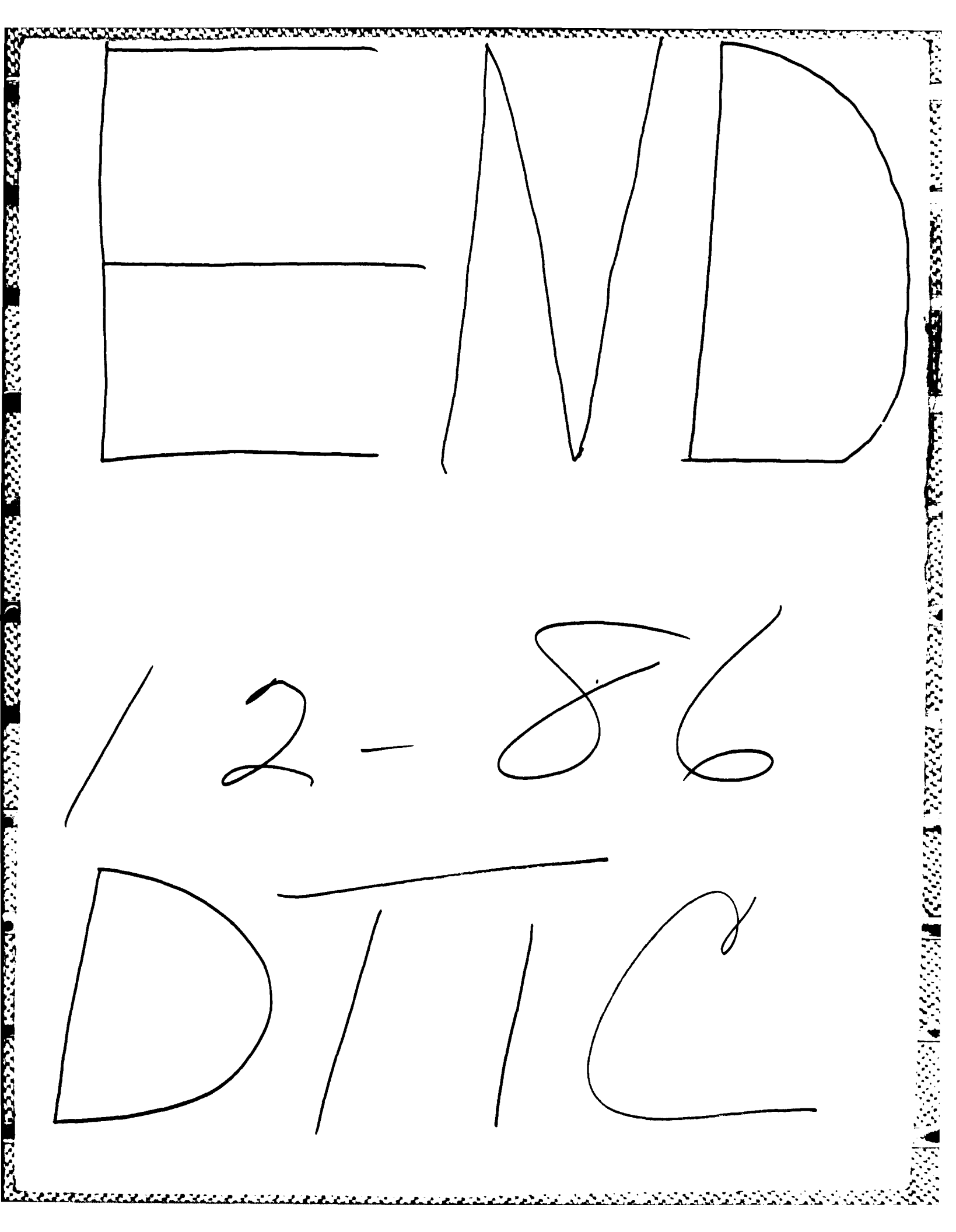
END
12-86
DTIC